The zebrafish mutant *dreammist* implicates sodium homeostasis in sleep regulation

Ida L. Barlow[1,2], Eirinn Mackay[1,3], Emily Wheater[1,4], Aimee Goel[1], Sumi Lim[1], Steve Zimmerman[5], Ian Woods[6], David A. Prober[7], and Jason Rihel[1,*]

[1] Department of Cell and Developmental Biology, University College London, UK;

[2] Current address: MRC London Institute for Medical Sciences, Imperial College London, UK

[3] Current address: Sainsbury Wellcome Centre for Neural Circuits and Behaviour, University College London, UK

[4] Current address: MRC centre for Reproductive Health, University of Edinburgh, UK

[5] Department of Molecular and Cellular Biology, Harvard University, USA

[6] Ithaca College, New York, USA

[7] Division of Biology and Biological Engineering, California Institute of Technology, Pasadena, USA

* Lead author: Jason Rihel j.rihel@ucl.ac.uk

Significance statement: Sleep is an essential behavioral state, but the genes that regulate sleep and wake states are still being uncovered. A viral insertion screen in zebrafish identified a novel sleep mutant called *dreammist*, in which a small, highly-conserved transmembrane protein is disrupted. The discovery of *dreammist* highlights the importance of a class of small transmembrane-protein modulators of the sodium pump in setting appropriate sleep duration.

ABSTRACT

Sleep is a nearly universal feature of animal behaviour, yet many of the molecular, genetic, and neuronal substrates that orchestrate sleep/wake transitions lie undiscovered. Employing a viral insertion sleep screen in larval zebrafish, we identified a novel gene, *dreammist* (*dmist*), whose loss results in behavioural hyperactivity and reduced sleep at night. The neuronally expressed *dmist* gene is conserved across vertebrates and encodes a small single-pass transmembrane protein that is structurally similar to the Na^+,K^+-ATPase regulator, FXYD1/Phospholemman. Disruption of either *fxyd1* or *atp1a3a*, a Na^+,K^+-ATPase alpha-3 subunit associated with several heritable movement disorders in humans, led to decreased night-time sleep. Since *atpa1a3a* and *dmist* mutants have elevated intracellular Na^+ levels and non-additive effects on sleep amount at night, we propose that Dmist-dependent enhancement of Na^+ pump function modulates neuronal excitability to maintain normal sleep behaviour.

INTRODUCTION

The ability of animals to switch between behaviourally alert and quiescent states is conserved across the animal kingdom (Cirelli, 2009; Joiner, 2016). Fundamental processes that govern the regulation of sleep-like states are shared across species, such as the roles of circadian and homeostatic cues in regulating the time and amount of sleep, stereotyped postures, heightened arousal thresholds, and the rapid reversibility to a more alert state (Joiner, 2016). The near ubiquity of sleep implies that it serves ancient functions and is subject to conserved regulatory processes. However, many key molecular components that modulate sleep and wake states remain undiscovered.

Over the past two decades, investigations into sleep and arousal states of genetically tractable model organisms, such as *Drosophila melanogaster*, *C. elegans*, and *Danio rerio* (zebrafish) have uncovered novel molecular and neuronal components of sleep regulation

through gain- and loss-of-function genetic screens (reviewed in Barlow and Rihel, 2017; Sehgal and Mignot, 2011). The power of screening approaches is perhaps best exemplified by the first forward genetic sleep screen, which identified the potassium channel *shaker* as a critical sleep regulator in *Drosophila* (Cirelli et al., 2005). This result continues to have a lasting impact on the field, as not only did subsequent sleep screening efforts uncover the novel Shaker regulator *sleepless*, (Koh et al., 2009), but investigations into Shaker's beta subunit Hyperkinetic ultimately revealed a critical role for this redox sensor linking metabolic function to sleep (Bushey et al., 2007; Kempf et al., 2019).

Disparate screening strategies across model organisms continue to unveil novel sleep modulators in both invertebrate and vertebrate model systems. For example, the roles of RFamide receptor DMSR-1 in stress-induced sleep in *C. elegans* (Iannacone et al., 2017) and SIK3 kinase in modulating sleep homeostasis in mice (Funato et al., 2016) were identified in genetic screens. Moreover, a gain of function screening strategy in *Drosophila* revealed the novel sleep and immune regulator, *nemuri* (Toda et al., 2019), and a zebrafish overexpression screen uncovered the secreted neuropeptides neuromedin U and neuropeptide Y, which decrease and increase sleep, respectively (Chiu et al., 2016; Singh et al., 2017). The success of screening strategies in revealing novel sleep-wake regulatory genes suggests that more sleep signals likely remain to be discovered.

One of the lessons from these genetic screens is that many of the uncovered genes play conserved roles across species. For example, Shaker also regulates mammalian sleep (Douglas et al., 2007) and RFamides induce sleep in worms, flies, and vertebrates (Lee et al., 2017; Lenz et al., 2015). Nevertheless, not every invertebrate sleep-regulatory gene has a clear vertebrate homolog, while some human sleep/wake regulators, such as the narcolepsy-associated neuropeptide hypocretin/orexin (Chemelli et al., 1999; Lin et al., 1999; Peyron et al., 2000; Sakurai, 2013), lack invertebrate orthologs. Therefore, genetic sleep screens in

74 vertebrates are likely to provide added value in uncovering additional regulatory components
75 required to control the initiation and amount of sleep in humans.

76 While sleep screening in mammals is feasible (Funato et al., 2016), it remains an expensive
77 and technically challenging endeavour. With its genetic tractability, availability of high-
78 throughput sleep assays (Rihel and Schier, 2013), and conserved sleep genetics, such as the
79 hypocretin, melatonin, locus coeruleus, and raphe systems (Gandhi et al., 2015; Singh et al.,
80 2015; Oikonomou et al., 2019; Prober et al., 2006), the larval zebrafish is an attractive
81 vertebrate system for sleep screens. We took advantage of a collection of zebrafish lines that
82 harbour viral-insertions in >3500 genes (Varshney et al., 2013) to perform a targeted genetic
83 screen. We identified a short-sleeping mutant, *dreammist*, with a disrupted novel, highly
84 conserved vertebrate gene that encodes a small single pass transmembrane protein.
85 Sequence and structural homology to the Na^+/K^+ pump regulator FXYD1/Phospholemman
86 suggests that Dreammist is a neuronal-expressed member of a class of sodium pump
87 modulators that is important for regulating sleep-wake behaviour.

RESULTS

Reverse genetic screen identifies *dreammist,* a mutant with decreased sleep

We used the 'Zenemark' viral-insertion based zebrafish gene knock-out resource (Varshney et al., 2013) to perform a reverse genetic screen to identify novel vertebrate sleep genes. This screening strategy offers several advantages compared to traditional chemical mutagenesis-based forward genetic screening approaches. First, unlike chemical mutagenesis, which introduces mutations randomly, viral insertions tend to target the 5' end of genes, typically causing genetic loss of function (Sivasubbu et al., 2007). Second, because the virus sequence is known, it is straightforward to map and identify the causative gene in mutant animals. Finally, since viral insertions in the Zenemark collection are already mapped and sequenced, animals harbouring insertions within specific gene classes can be selected for testing (Figure S1A). This allowed us to prioritise screening of genes encoding protein classes that are often linked to behaviour, such as G-protein coupled receptors, neuropeptide ligands, ion channels, and transporters (Supplemental Data 1).

For screening, we identified zebrafish sperm samples from the Zenemark collection (Varshney et al., 2013) that harboured viral insertions in genes of interest and used these samples for *in vitro* fertilization and the establishment of F2 families, which we were able to obtain for 26 lines. For each viral insertion line, clutches from heterozygous F2 in-crosses were raised to 5 days post-fertilisation (dpf) and tracked using videography (Figure S1A) to quantify the number and duration of sleep bouts (defined in zebrafish larvae as inactivity lasting 1 minute or longer; Prober et al., 2006) and waking activity (time spent moving per active bout) over 48 hours. The genotypes of individual larvae were determined by PCR after behavioural tracking, with each larva assigned as wild type, heterozygous, or homozygous for a given viral insertion to assess the effect of genotype on sleep/wake behaviour. While most screened heterozygous and homozygous lines had minimal effects on sleep-wake behavioural

parameters (Figure S1B-S1C), one homozygous viral insertion line, *10543/10543,* had a reduction in daytime sleep (Figure S1B) and an increase in daytime waking activity (Figure S1C) relative to their wild type sibling controls. We re-named this *10543* viral insertion line *dreammist* (*dmist*).

In follow-up studies, we observed that animals homozygous for the viral insertion at this locus (*dmist*$^{vir/vir}$) showed a decrease in sleep during the day and a trend to sleep less at night compared to their wild-type siblings (*dmist*$^{+/+}$) (Figure 1A). *dmist* mutants had an almost 50% reduction in the average amount of daytime sleep (Figure 1C) due to a decrease in the number of sleep bouts (Figure 1D), whereas the sleep bout length at night was significantly reduced (Figure 1E). *dmist*$^{vir/vir}$ larvae also exhibited significantly increased daytime waking activity, which is the locomotor activity while awake (Figure 1B, 1F). Because Zenemark lines can contain more than one viral insertion (17.6% of lines have ≥2 insertions; Varshney et al 2013), we outcrossed *dmist*$^{vir/+}$ fish to wild-type fish of the AB-TL background and re-tested *dmist* mutant fish over several generations. Normalising all the behavioural parameters to *dmist*$^{+/+}$ controls with a linear mixed effects (LME) model showed consistent sleep changes in *dmist*$^{vir/vir}$ fish over 5 independent experiments (Figure 1G). The *dmist*$^{vir/vir}$ larvae consistently show a more than 50% decrease in sleep during the day due to a significant reduction in the number and duration of sleep bouts, as well as a large increase in waking activity (Figure 1G). The *dmist*$^{vir/vir}$ mutants also had a significant reduction in sleep at night compared to wild type siblings (Figure 1G). These effects on sleep and wakefulness are not due to alterations in circadian rhythms, as behavioural period length in fish that were entrained and then shifted to free-running constant dark conditions was unaffected in *dmist*$^{vir/vir}$ compared to wild-type sibling larvae (Figure S2A-S2C).

The *dmist* gene encodes a novel, small transmembrane protein

Having identified a sleep mutant, we next sought to investigate the target gene disrupted by the viral insertion. Line *10543* (*dmist*^{vir}) was initially selected for screening due to a predicted disruption of a gene encoding a serotonin transporter (*slc6a4b*) on chromosome 5. However, mapping of the *dmist* viral insertion site by inverse-PCR and sequencing revealed that the virus was instead inserted into the intron of a small two-exon gene annotated in the Zv6 genome assembly as a long intergenic non-coding RNA (lincRNA; gene transcript ENSDART00000148146, gene name *si:dkey234h16.7*), which lies approximately 6 kilobases (kb) downstream of the *slc6a4b* gene in zebrafish. At least part of this region is syntenic across vertebrates, with a small two-exon gene identified adjacent to the genes *ankrd13a* and *GIT* in several vertebrates, including human and mouse (Figure 2A). Amplifying both 5' and 3' ends of zebrafish *si:dkey234h16.7* and mouse E13.5 *1500011B03-001* transcripts with Rapid Amplification of cDNA ends (RACE) confirmed the annotated zebrafish and mouse transcripts and identified two variants with 3' untranslated regions (3'UTR) of different lengths in zebrafish (Figure S3B). To test whether the viral insertion in *dmist*$^{vir/vir}$ disrupts expression of *si:dkey234h16.7* or neighbouring genes, we performed quantitative analysis of gene transcript levels in wild type and mutant *dmist* larvae by RT-qPCR. This revealed that the *dmist* viral insertion caused a more than 70% reduction in the expression of *si:dkey234h16.7* while the expression of the most proximal 5' or 3' flanking genes, *slc6a4b_Dr* and *ankrd13a_Dr*, were unaffected (Figure 2B and S3A). Since this reduced expression is most consistent with *si:dkey234h16.7* being the causal lesion of the *dmist* mutant sleep phenotype, we renamed this gene *dreammist* (*dmist*).

Computational predictions indicated that the *dmist* transcripts contain a small open reading frame (ORF) encoding a protein of 70 amino acids (aa) (Figure 2C). Querying the human and vertebrate protein databases by BLASTp using the C-terminal protein sequence of Dmist identified orthologs in most vertebrate clades, including other species of teleost fish, birds,

amphibians, and mammals (Figure 2A, C). All identified orthologs encoded predicted proteins with an N-terminal signal peptide sequence and a C-terminal transmembrane domain (Figure 2C). The peptide sequence identity across orthologs ranged from 38 to 84%, with three peptide motifs (QNLV, CVYKP, RRR) showing high conservation across all vertebrates, and high similarity for many additional residues (Figure 2C, Figure S3D). Additional searches by tBLASTn failed to identify any non-vertebrate *dmist* orthologs. In summary, we found that the *dreammist* gene, the expression of which is disrupted in *dmist*$^{vir/vir}$ fish with sleep phenotypes, encodes a protein of uncharacterized function that is highly conserved across vertebrates at both the genomic and molecular levels.

Genetic molecular analysis of *dmist* expression in zebrafish and mouse

Because the viral insertion disrupts *dmist* throughout the animal's lifetime, we examined both the developmental and spatial expression of *dmist* to assess when and where its function may be required for normal sleep. Using the full-length transcript as a probe (Figure S3B), we performed *in situ* hybridization across embryonic and larval zebrafish development. Maternally deposited *dmist* was detected in early embryos (2-cell stage) prior to the maternal to zygotic transition (Giraldez et al., 2006) (Figure 2D). Consistent with maternal deposition of *dmist* transcripts, inspection of the 3' end of the *dmist* gene revealed a cytoplasmic polyadenylation element ('TTTTTTAT'; Supplemental Information 2) that is required for zygotic translation of maternal transcripts (Villalba et al., 2011). At 24 hpf, transcripts were detected in regions that form the embryonic brain, such as ventral telencephalon, diencephalon and cerebellum, and in the developing eye (Figure 2D, S3C). By 5 dpf, *dmist* transcripts were detected throughout the brain (Figure 2D). To test whether *dmist* transcripts are under circadian regulation, we performed RT-qPCR in fish that were entrained and then shifted to free-running constant dark conditions. In contrast with the robust 24-hr rhythmic transcription of the circadian clock gene

188 *per1*, we did not detect any changes in *dmist* expression throughout the 24 hour circadian cycle
189 (Figure S2D).

190 Consistent with brain expression in larval zebrafish, we identified the expression of
191 *Dmist_Mm* in a published RNAseq dataset of six isolated cell types from mouse cortex (Zhang
192 et al., 2014). We confirmed that *Dmist_Mm* is specifically enriched in neurons by hierarchical
193 clustering of all 16,991 expressed transcripts across all six cells types, which demonstrated
194 that *Dmist_Mm* co-clusters with neuronal genes (Figure S3E). Pearson correlation of
195 *Dmist_Mm* with canonical markers for the six cell types showed that *Dmist_Mm* expression is
196 highly correlated with other neuronal genes but not genes associated with microglia,
197 oligodendrocytes, or endothelia. This result indicates that *dmist* is specifically expressed in
198 neurons in both zebrafish and mouse (Figure S3F).

199

200 **Dmist localises to the plasma membrane**

201 Although the *dmist* gene encodes a conserved ORF with a predicted signal peptide
202 sequence and transmembrane domain (Figure 2C; Figure S3G-I), we wanted to confirm this
203 small peptide can localise to the membrane and if so, on which cellular compartments. To test
204 these computational predictions, we transiently co-expressed GFP-tagged Dmist (C-terminal
205 fusion) with a marker for the plasma membrane (myr-Cherry) in zebrafish embryos. Imaging at
206 90% epiboly revealed Dmist-GFP localised to the plasma membrane (Figure 2E). Conversely,
207 introducing a point mutation into Dmist's signal peptide cleavage site (DmistA22W-GFP)
208 prevented Dmist from trafficking to the plasma membrane, with likely retention in the
209 endoplasmic reticulum (Figure 2F). Together, these data indicate that Dmist localises to the
210 plasma membrane despite its small size, as computationally predicted.

211

212 **CRISPR/Cas9 generated *dmist^{i8}* mutant exhibits decreased night-time sleep**

dmist expression was reduced by 70% in the viral insertion line, suggesting that *dmist*^{vir} is a hypomorphic allele. To confirm that the sleep phenotypes observed in *dmist*$^{vir/vir}$ animals are due to the loss of Dmist function, we used CRISPR/Cas9 to create an independent *dmist* loss of function allele. We generated a zebrafish line in which the *dmist* gene contains an 8 bp insertion that causes a frameshift and early stop codon (*dmist*^{i8}, Figure 3A). The *dmist*^{i8} allele is predicted to encode a truncated protein lacking the complete signal peptide sequence and transmembrane domain (Figure 3B), indicating this is likely a null allele. RT-qPCR showed that *dmist* transcript levels were 60% lower in *dmist*$^{i8/i8}$ fish compared to wild type siblings, consistent with nonsense-mediated decay (Figure S4A, B) (Wittkopp et al., 2009).

We next assessed the sleep and activity patterns of *dmist*$^{i8/i8}$ fish. As seen in exemplar individual tracking experiments, *dmist*$^{i8/i8}$ larvae sleep less at night due to fewer sleep bouts and also show an increase in waking activity relative to wild type and heterozygous mutant siblings (Figure 3C-H). This significant night-time reduction in sleep and increase in hyperactivity is also apparent when combining 5 independent experiments with a linear mixed effects (LME) model to normalize behaviour across datasets (Figure 3I). Although *dmist*$^{vir/vir}$ larvae also sleep less at night (Figure 1G), the large day-time reduction in sleep observed in *dmist*$^{vir/vir}$ larvae is absent in *dmist*$^{i8/i8}$ animals, perhaps due to differences in genetic background that affect behaviour. Because the *dmist*^{vir} is likely a hypomorphic allele, we focused subsequent experiments on the CRISPR-generated *dmist*$^{i8/i8}$ larvae.

To test whether the increased night-time activity of *dmist*$^{i8/i8}$ mutants persists in older animals, we raised *dmist*$^{i8/i8}$ mutants with their heterozygous and wild type siblings to adulthood in the same tank and tracked individual behaviour for several days on a 14:10 light:dark cycle. As in larval stages, *dmist*$^{i8/i8}$ adults were hyperactive relative to both *dmist*$^{i8/+}$ and *dmist*$^{+/+}$ siblings, maintaining a higher mean speed at night (Figure 3J-L). This suggests that either Dmist affects a sleep/wake regulatory circuit during development that is permanently altered in

238 *dmist* mutants, or that Dmist is continuously required to maintain normal levels of night-time
239 locomotor activity.

240

241 **Dmist is distantly related to the Na^+/K^+ pump regulator Fxyd1 (Phospholemman)**

242 Because Dmist is a small, single pass transmembrane domain protein without any clear
243 functional motifs and has not been functionally characterized in any species, we searched for
244 similar peptides that might provide clues for how Dmist regulates behaviour. Using the multiple
245 sequence alignment tool MAFFT to align the zebrafish, mouse, and human Dmist peptides
246 (Katoh and Toh, 2010) and seeding a hidden Markov model iterative search (JackHMMR) of
247 the Uniprot database (Johnson et al., 2010), we found distant homology between Dmist and
248 Fxyd1/Phospholemman (Figure 4A), a small transmembrane domain peptide that regulates ion
249 channels and pumps, including the Na^+,K^+-ATPase pump (Crambert et al., 2002). Dmist and
250 Fxyd1 share 27-34% amino acid homology, including an RRR motif at the C-terminal end,
251 although Dmist lacks a canonical FXYD sequence (Figure 4A). In addition, computational
252 predictions using the AlphaFold protein structure database revealed structural similarities
253 between Dmist and Fxyd1 (Jumper et al., 2021), suggesting that Dmist may belong to a class
254 of small, single pass transmembrane ion pump regulators.

255 Using *In situ* hybridisation, we found that *fxyd1* is expressed in cells along the brain ventricle
256 and choroid plexus (Figure 4C) in contrast to the neuronal expression of *dmist* (Figure 2D).
257 Despite these different expression patterns, based on their sequence similarity we reasoned
258 that Fxyd1 and Dmist may regulate the same molecular processes that are involved in sleep.
259 To test this hypothesis, we used CRISPR/Cas9 to generate a 28 bp deletion in the third exon
260 of the zebrafish *fxyd1* gene, causing a frameshift that is predicted to encode a truncated protein
261 that lacks the FXYD, transmembrane, and C-terminal domains (Figure 4B). Contrary to a
262 previous report based on morpholino knockdown (Chang et al., 2012), *fxyd1*$^{\Delta 28/\Delta 28}$ larvae were

viable with no detectable defect in inflation of the brain ventricles. We therefore tested *fxyd1* mutant larvae for sleep phenotypes. Like *dmist* mutants, *fxyd1*$^{\Delta 28/\Delta 28}$ larvae slept less at night (Figure 4D-F). Interestingly, this sleep loss is mainly due to shorter sleep bouts (Figure 4F), indicating that *fxyd1* mutants initiate sleep normally but do not properly maintain it, unlike *dmist* mutants, which initiate fewer night-time sleep bouts, although in both cases there is consolidation of the wake state at night (Figure 3I, 4F). Thus, despite the non-neuronal expression of *fxyd1* in the brain, mutation of the gene most closely related to *dmist* results in a similar sleep phenotype.

The brain-wide Na^+/K^+ pump alpha subunit Atp1a3a regulates sleep at night

Given the similarity between Dmist and Fxyd1 and their effects on night-time sleep, we hypothesized that mutations in Na^+/K^+ pump subunits known to interact with Fxyd1 might also affect sleep. Consistent with this hypothesis, a low dose of the Na^+/K^+ pump inhibitor, ouabain, reduced night-time sleep in dose-response studies (Figure S5A). When applied in the late afternoon of 6 dpf, 1 µM ouabain decreased subsequent night-time sleep by 16.5% relative to controls, an effect size consistent with those observed in *dmist* mutants (Figure 5A, C). Night-time waking activity was also significantly increased after low-dose ouabain exposure (Figure 5B, D). Ouabain binds to specific sites within the first extracellular domain of Na^+/K^+ pump alpha subunits (Price and Lingrel, 1988), and species-specific changes to these sites confers species-specific ouabain resistance, as in the case of two naturally occurring amino acid substitutions present in the Atp1a1 subunit of mice (Dostanic et al., 2004). Alignment of the ouabain sensitive region of zebrafish and mouse Na^+/K^+ pump alpha subunits revealed that zebrafish Atp1a1a lacks the conserved Glutamine at position 121 (Figure 5E), suggesting that one of the other subunits with conserved ouabain-binding sites is responsible for the low dose ouabain sleep effects. We focused on the Na^+/K^+ pump alpha-3 subunit (Atp1a3), as this has

been shown to directly interact with Fxyd1 in mammalian brain tissue (Feschenko et al., 2003). Murine *Dmist* expression also correlates well with the *Atp1a3* distribution across 5 brain cell types in mouse (Pearson correlation coefficient = 0.63), which has the strongest correlation score with neuronal markers (Figure S5B compared to Figure S3F). In contrast, zebrafish *atp1a2a* is reportedly expressed in muscle at larval stages, while *atp1a1b* is confined to cells along the ventricle (Thisse et al., 2001).

Zebrafish have two Atp1a3 paralogs, *atp1a3a* and *atp1a3b*. Similar to *dmist*, *atp1a3a* is widely expressed in the larval zebrafish brain (Figure 5F, compare to Figure 2D). While *atp1a3b* is also expressed in the zebrafish brain, its expression is more limited to regions of the midbrain and hindbrain (Figure S5C). To test whether these genes are involved in regulating zebrafish sleep, we used CRISPR/Cas9 to isolate an allele of *atp1a3a* containing a 19 bp deletion and an allele of *atp1a3b* containing a 14 bp deletion. Both mutations are predicted to generate null alleles due to deletion of the start codon (Figure 5G, S5D). Both *atp1a3a*$^{\Delta 19/\Delta 19}$ and *atp1a3b*$^{\Delta 14/\Delta 14}$ mutant larvae were healthy and viable through early development, although *atp1a3b* mutant larvae were not obtained at Mendelian ratios (55 wild type [52.5 expected], 142 [105] *atp1a3b*$^{+/-}$, 13 [52.5] *atp1a3b*$^{-/-}$; $p<0.0001$, Chi-squared), suggesting some impact on early stages of development leading to lethality. Contrary to a previous report based on morpholino injections (Doğanli et al., 2013), neither mutant had defects in the inflation of their brain ventricles. Sleep-wake tracking experiments found that *atp1a3b*$^{\Delta 14/\Delta 14}$ mutants were more active during the day with minimal sleep phenotypes (Figure S5E-G). In contrast, mutation of *atp1a3a* resulted in large effects on sleep-wake behaviour. Compared to wild type and heterozygous mutant siblings, *atp1a3a*$^{\Delta 19/\Delta 19}$ animals were hyperactive throughout the day and night and had a large reduction in sleep at night (Figure 5H, I). The night-time sleep reduction was due to a reduction in the length of sleep bouts, as *atp1a3a* mutants even had a small increase in the number of sleep bouts at night (Figure 5J). In conclusion, loss of *atp1a3a* results

in sleep loss at night, similar to treatment with the small molecule *ouabain*, and to *dmist* and *fxyd1* mutants. Notably, the *atp1a3a* mutant phenotype is much stronger, as might be expected if Dmist plays a modulatory, and Atp1a3a a more central, role in Na^+/K^+ pump activity.

Dmist modulates Na^+/K^+ pump function and neuronal activity-induced sleep homeostasis

The similar night-time reduction in sleep in *dmist* and *atp1a3a* mutants, combined with the similarities between Dmist and Fxyd1, suggested that Dmist may regulate the Na^+/K^+ pump. We therefore exposed wild type and mutant larvae to pentylenetetrazol (PTZ), a GABA-receptor antagonist that leads to globally heightened neuronal activity and elevated intracellular sodium levels that must be renormalized by Na^+/K^+ pump activity. Consistent with the hypothesis that Dmist and Atp1a3a subunits are important for a fully functional Na^+/K^+ pump, brains from both $dmist^{i8/i8}$ and $atp1a3a^{\Delta 19/\Delta 19}$ larvae had elevated intracellular sodium levels after exposure to PTZ (Figure 6A). Thus, neither *dmist* nor *atp1a3a* mutants were able to restore intracellular sodium balance after sustained neuronal activity as quickly as wild type siblings. Consistent with the night-specific alterations in sleep behaviour, we also found that baseline brain Na^+ levels in *dmist* mutants were significantly elevated at night but not during the day (Figure 6B). Collectively, these data are consistent with the hypothesis that night-time sleep duration is affected by changes in Na^+/K^+ pump function and that Dmist is required to maintain this function both at night and after sustained high levels of neuronal activity.

We have previously shown in zebrafish that a brief exposure to hyperactivity-inducing drugs such as the epileptogenic PTZ or wake-promoting caffeine induces a dose-dependent increase in homeostatic rebound sleep following drug washout that is phenotypically and mechanistically similar to rebound sleep following physical sleep deprivation (Reichert et al., 2019). Based on

their exaggerated intracellular Na^+ levels following exposure to PTZ, we predicted that *dmist* mutants would also have increased rebound sleep in response to heightened neuronal activity. Upon wash-on/wash-off of lower dose (5 mM) PTZ, sleep rebound occurs in approximately 50% of wild type larvae (Reichert et al., 2019; Figure 6C, D). In contrast, all *dmist*$^{i8/i8}$ larvae showed increased rebound sleep compared to *dmist*$^{+/+}$ sibling controls (Figure 6C-E). Taken together with the elevated sodium retention experiments, such increases in rebound sleep induced by neuronal activity suggests that *dmist*$^{i8/i8}$ fish more rapidly accumulate sleep pressure in response to heightened neuronal activity.

Finally, we predicted that if Dmist is affecting baseline sleep via modulation of Atp1a3a-containing Na^+/K^+ pumps, *dmist*$^{-/-}$; *atp1a3a*$^{-/-}$ double mutants should have a reduction in night-time sleep that is not the sum of effects from either mutant alone. In other words, if Dmist and Atp1a3a are acting in separate pathways, the double mutant would have an additive phenotype, but if Dmist and Atp1a3a act together in the same complex/pathway, the mutant phenotypes should be non-additive. Indeed, *dmist*$^{-/-}$; *atp1a3a*$^{-/-}$ mutants have a sleep reduction similar to that of *atp1a3a*$^{-/-}$ mutants alone, consistent with a non-additive effect (Figure 6F and S6). Similar non-additivity can be also observed in the *dmist*$^{-/-}$; *atp1a3a*$^{+/-}$ animals, which, like *atp1a3a*$^{+/-}$ animals alone, have a milder sleep reduction, indicating that the lack of additivity between dmist and atp1a3a phenotypes is unlikely due to a floor effect, since double homozygous mutants can sleep even less (Figure 6F). This genetic interaction data is consistent with our hypothesis that Atp1a3a and Dmist act in the same pathway—the Na^+/K^+ pump-- to influence sleep.

DISCUSSION

Genetic screening discovers *dmist*, a novel sleep-regulatory gene

Using a reverse genetic viral screening strategy, we discovered a short-sleeping mutant, *dmist*, which has a disruption in a previously uncharacterized gene encoding a small transmembrane peptide. Given that the *dmist* mutant appeared within the limited number of 26 lines that we screened, it is likely that many other sleep genes are still waiting to be discovered in future screens. In zebrafish, one promising screening strategy will be to employ CRISPR/Cas9 genome editing to systematically target candidate genes. Advances in the efficiency of this technology now makes it feasible to perform a CRISPR "F0 screen" in which the consequences of bi-allelic, gene-specific mutations are rapidly tested in the first generation, with only the most promising lines pursued in germline-transmitted mutant lines (Grunwald et al., 2019; Jao et al., 2013; Kroll et al., 2021; Shah et al., 2015; Shankaran et al., 2017; Wu et al., 2018). CRISPR F0 screens could be scaled to systematically target the large number of candidate sleep-regulatory genes identified through human GWAS studies and sequencing of human patients suffering from insomnia and neuropsychiatric disorders (Allebrandt et al., 2013; Dashti et al., 2019; Jansen et al., 2019; Jones et al., 2019; Lane et al., 2019; Lek et al., 2016; Palagini et al., 2019).

Dmist is related to the Na+/K+ pump regulator Fxyd1

The small Dmist transmembrane protein is highly conserved across vertebrates, expressed in neurons, and important for maintaining normal sleep levels. How can such a small, single pass transmembrane protein lacking any clear functional domains modulate the function of neurons and ultimately animal behaviour? The recognition that Dmist has sequence homology (~35% amino acid similarity; a conserved 'RRR' motif in the C-terminus) and structural homology (e.g. signal peptide and single pass transmembrane domains) to the Na^+,K^+-ATPase pump regulator Fxyd1 (Phospholemman) offers some important clues.

Fxyd1/Phospholemman is a member of the FXYD protein family, of which there are seven mammalian members (Sweadner and Rael, 2000). Each of the FXYD proteins is small, contains a characteristic FXYD domain, and has a single transmembrane domain. FXYD family members interact with alpha subunits of the Na^+,K^+ ATPase to regulate the function of this pump, with individual family members expressed in different tissues to modulate Na^+,K^+-ATPase activity depending on the physiological needs of the tissue (Geering et al., 2003). In cardiac muscle, FXYD1 is thought to act as a hub through which various signalling cascades, such as PKA, PKC, or nitric oxide, can activate or inhibit Na^+ pump activity (Pavlovic et al., 2013). For example, FXYD1 is critical for mediating the increased Na^+ pump activity observed after β-receptor stimulation via cAMP-PKA signalling (Despa et al., 2008). Much less is known about the role of FXYD1 in non-cardiac tissue, although it is expressed in neurons in the mammalian cerebellum, the choroid plexus, and ependymal cells, where it interacts with all three alpha subunits of the Na^+,K^+ ATPase (Feschenko et al., 2003).

In zebrafish, we also found that *fxyd1* is expressed in cells around the ventricles and in the choroid plexus (Figure 4C), in contrast to *dmist* which is expressed in neurons throughout the brain. Despite the different expression patterns, mutation of each gene resulted in a similar reduction of sleep at night. However, unlike *dmist* mutants, which have fewer sleep bouts (i.e. initiate sleep less) and an increase in waking locomotor activity, *fxyd1* mutants have shorter sleep bouts (i.e. cannot maintain sleep) on average and do not have a locomotor activity phenotype. Just as the various FXYD family members modulate the Na^+/K^+ pump in different tissue- and context-specific ways, this phenotypic variation between *fxyd1* and *dmist* mutants could be due to the different *fxyd1* and *dmist* expression patterns, modulation kinetics of pump/channel dynamics, or interaction with different accessory proteins or signal transduction cascades. Nevertheless, the similar timing and magnitude of sleep reduction, combined with

409 the structural similarity of Fxyd1 and Dmist, suggest that they may regulate similar sleep-
410 related processes.

411

412 **Dmist, the sodium pump, and sleep**

413 The similarity between Dmist and FXYD1 led us to directly manipulate the Na^+,K^+ ATPase
414 to test its importance in sleep. The Na^+,K^+-ATPase is the major regulator of intracellular Na^+ in
415 all cells and, by actively exchanging two imported K^+ ions for three exported Na^+ ions, is
416 essential for determining cellular resting membrane potential (reviewed in Clausen et al.,
417 2017). The Na^+,K^+-ATPase consists of a catalytic alpha subunit (4 known isoforms, ATP1A1-
418 4), a supporting beta subunit (3 isoforms, ATP1B1-3), and a regulatory gamma subunit (the
419 FXYD proteins). The alpha1 and alpha3 subunits are the predominant catalytic subunits in
420 neurons (alpha2 is mostly restricted to glia), although the alpha1 subunit is also used
421 ubiquitously in all tissues (McGrail et al., 1991). By mutating zebrafish orthologs of *Atp1a3*, we
422 therefore could test the neuronal-specific role of the Na^+,K^+-ATPase in sleep.

423 Mutations in both zebrafish *Atp1a3* orthologs increased waking locomotor behaviour during
424 the day. However, only mutations in *atp1a3a,* which is expressed brain-wide, but not in
425 *atp1a3b*, which is expressed in more restricted brain regions, led to changes in night-time
426 sleep. The *atp1a3a* mutants have a larger sleep reduction than $dmist^{vir}$, $dmist^{i8}$, or $fxyd1^{\Delta 28}$
427 mutants, which is expected since loss of a pump subunit should have a larger effect than the
428 loss of a modulatory subunit, as has been shown for other ion channels (Cirelli et al., 2005;
429 Wu et al., 2014). Autosomal dominant missense mutations leading to loss of function in
430 *ATP1A3* cause movement disorders such as rapid-onset dystonia parkinsonism and childhood
431 alternating hemiplegia (recurrent paralysis on one side) in humans (Canfield et al., 2002;
432 Heinzen et al., 2014), while loss of function mutations in *Atp1a3* result in generalised seizures

and locomotor abnormalities, including hyperactivity, in mice, which was not observed in zebrafish (Clapcote et al., 2009; Hunanyan et al., 2015; Ikeda et al., 2013; Kirshenbaum et al., 2011; Sugimoto et al., 2014). A very high prevalence of insomnia was recently reported in patients with childhood alternating hemiplegia, some of which harboured mutations in *Atp1a3* (Kansagra et al., 2019), consistent with our observations that insomnia at night is a direct behavioural consequence of *atp1a3a* mutation in zebrafish. Since zebrafish *atp1a3a* mutants phenocopy the insomnia and hyperactivity phenotypes observed in patients, small molecule screens aimed at ameliorating zebrafish *atp1a3a* mutant phenotypes may be a promising approach for the rapid identification of new therapies for the management of this disease (Hoffman et al., 2016; Rihel et al., 2010).

Together, the night-specific sleep phenotypes of *dmist*, *fxyd1*, and *atp1a3a* mutants point to a role for the Na^+,K^+-ATPase in boosting sleep at night. How might the alpha3 catalytic subunit of the Na^+/K^+ pump regulate sleep, and how could Dmist be involved? We found that Dmist is required for proper maintenance of brain intracellular Na^+ levels at night but not during the day, mirroring the timing of sleep disruption in *dmist*$^{i8/i8}$ animals. This suggests that the decreased night-time sleep of *dmist* mutants is due to a specific requirement for Dmist modulation of the Na^+/K^+ pump at night. However, we cannot exclude the possibility that Dmist's function is required in only a subset of critical sleep/wake regulatory neurons during the day that then influence behaviour at night, such as the wake-active, sleep-homeostatic regulating serotonergic neurons of the raphe (Oikonomou et al., 2019) or wake-promoting Hcrt/orexin neurons (Li et al., 2022). We also cannot exclude a role for Dmist and the Na^+/K^+ pump in developmental events that impact sleep, although our observation that ouabain treatment, which inhibits the pump acutely after early development is complete, also impacts sleep, argues against a developmental role. Another possibility is that disruption of proper establishment of the Na^+ electrochemical gradient in *dmist* mutant neurons leads to dysfunction

458 of various neurotransmitter reuptake transporters, including those for glycine, GABA,
459 glutamate, serotonin, dopamine, and norepinephrine, which rely on energy from the Na^+
460 gradient to function (Kristensen et al., 2011).

461 A third possibility is that Dmist and the Na^+,K^+-ATPase regulate sleep not by modulation of
462 neuronal activity per se but rather via modulation of extracellular ion concentrations. Recent
463 work has demonstrated that interstitial ions fluctuate across the sleep/wake cycle in mice. For
464 example, extracellular K^+ is high during wakefulness, and cerebrospinal fluid containing the ion
465 concentrations found during wakefulness directly applied to the brain can locally shift neuronal
466 activity into wake-like states (Ding et al., 2016). Given that the Na^+,K^+-ATPase actively
467 exchanges Na^+ ions for K^+ , the high intracellular Na^+ levels we observe in *atp1a3a* and *dmist*
468 mutants is likely accompanied by high extracellular K^+. Although we can only speculate at this
469 time, a model in which extracellular ions that accumulate during wakefulness and then directly
470 signal onto sleep-regulatory neurons could provide a direct link between Na^+,K^+ ATPase
471 activity, neuronal firing, and sleep homeostasis. Such a model could also explain why
472 disruption of *fxyd1* in non-neuronal cells also leads to a reduction in night-time sleep.

473 In addition to decreased night-time sleep, we also observed that *dmist* mutants have an
474 exaggerated sleep rebound response following the high, widespread neuronal activity induced
475 by the GABA-receptor antagonist, PTZ. Since both Atp1a3a and Dmist were essential for re-
476 establishing proper brain intracellular Na^+ levels following PTZ exposure (Figure 6A), we
477 speculate that the exaggerated sleep rebound is a consequence of increased neuronal
478 depolarization due to defective Na^+ pump activity. This is consistent with our previous
479 observations that the intensity of brain-wide neuronal activity impacts the magnitude of
480 subsequent sleep rebound via engagement of the Galanin sleep-homeostatic output arm
481 (Reichert et al., 2019). Why does loss of *dmist* lead to both decreased night-time sleep and
482 increased sleep rebound in response to exaggerated neuronal activity during the day? One

possibility is that Na^+/K^+ pump complexes made up of different alpha and beta subunits may be differentially required for maintaining Na^+ homeostasis under physiological conditions and have different affinities for (or regulation by) Dmist. For example, the Atp1a1 subunit is considered the Na^+/K^+ pump workhorse in neurons, while Atp1a3, which has a lower affinity for Na^+ ions, plays an essential role in repolarizing neurons when Na^+ rapidly increases during high levels of neuronal activity, such as after a seizure (Azarias et al., 2013). If Dmist preferentially interacts with Atp1a3a subunit, with which the non-additive effect of *dmist* and *atp1a3a* mutation on sleep is consistent , day-time sleep-related phenotypes in *dmist* mutants might be uncovered only during physiological challenge. Conversely, neurons may be more dependent on Atp1a3a and Dmist for sodium homeostasis at night due to changes in Na^+/K^+ pump composition, Dmist interactions, or ion binding affinities. For example, activity of the Na^+/K^+ pump can be modulated by the circadian clock (Damulewicz et al., 2013; Nakashima et al., 2018), changes in substrate availability, including ATP (reviewed in Therien and Blostein, 2000), or hormones (Ewart and Klip, 1995). Teasing out how Dmist modulation of the Na+/K+ pump changes across the day-night cycle, and in which neurons Dmist's function may be particularly important at night, will require future investigation.

In conclusion, through a genetic screening strategy in zebrafish, we have identified a novel brain expressed gene that encodes a small transmembrane protein regulator of night-time sleep and wake behaviours. Future work will be required to uncover the precise signalling dynamics by which Dmist regulates the Na^+,K^+-ATPase and sleep.

Acknowledgements

The initial screen, discovery, and characterization of *dreammist* was conducted in the lab of Alexander F Schier at Harvard University. We also would like to thank members of the Rihel lab and other UCL zebrafish groups for helpful comments on experiments and the manuscript.

We thank Shannon Shibata-Germanos for *fxyd1* mutant tracking experiments, John Parnavalas for reagents, Christine Orengo for help with small peptide sequence searches, Stuart Peirson for early access to mouse transcriptomic data, and Finn Mango Bamber for the Pokémon-card inspired *dreammist* name. The work was funded by NIH grants awarded to Alexander Schier (GM085357 and HL10952505); an ERC Starting Grant (#282027) and Wellcome Trust Investigator Award (#217150/Z/19/Z) to JR; NIH grant R35 NS122172 to DAP; and a Grand Challenges PhD studentship to ILB.

REFERENCES

Aday, A.W., Zhu, L.J., Lakshmanan, A., Wang, J., and Lawson, N.D., 2011. Identification of cis regulatory features in the embryonic zebrafish genome through large-scale profiling of H3K4me1 and H3K4me3 binding sites. Dev. Biol. 357, 450–462. https://doi.org/10.1016/j.ydbio.2011.03.007

Allebrandt, K. V, Amin, N., Müller-Myhsok, B., Esko, T., Teder-Laving, M., Azevedo, R.V.D.M., Hayward, C., van Mill, J., Vogelzangs, N., Green, E.W., et al., 2013. A KATP channel gene effect on sleep duration: from genome-wide association studies to function in Drosophila. Mol. Psychiatry 18, 122–132. https://doi.org/10.1038/mp.2011.142

Azarias, G., Kruusmägi, M., Connor, S., Akkuratov, E.E., Liu, X.L., Lyons, D., Brismar, H., Broberger, C., and Aperia, A., 2013. A specific and essential role for Na,K-ATPase α3 in neurons co-expressing α1 and α3. J. Biol. Chem. 288, 2734–2743. https://doi.org/10.1074/jbc.M112.425785

Barlow, I.L., and Rihel, J., 2017. Zebrafish sleep: from geneZZZ to neuronZZZ. Curr. Opin. Neurobiol. 44, 65–71. https://doi.org/10.1016/j.conb.2017.02.009

Bushey, D., Huber, R., Tononi, G., and Cirelli, C., 2007. Drosophila Hyperkinetic mutants have reduced sleep and impaired memory. J. Neurosci. 27, 5384–93. https://doi.org/10.1523/JNEUROSCI.0108-07.2007

Canfield, V.A., Loppin, B., Thisse, B., Thisse, C., Postlethwait, J.H., Mohideen, M.-A.P.., Rajarao, S.J.R., and Levenson, R., 2002. Na,K-ATPase α and β subunit genes exhibit unique expression patterns during zebrafish embryogenesis. Mech. Dev. 116, 51–59.

https://doi.org/10.1016/S0925-4773(02)00135-1

Chang, J.T., Lowery, L.A., and Sive, H., 2012. Multiple roles for the Na,K-ATPase subunits, Atp1a1 and Fxyd1, during brain ventricle development. Dev. Biol. 368, 312–22. https://doi.org/10.1016/j.ydbio.2012.05.034

Chemelli, R.M., Willie, J.T., Sinton, C.M., Elmquist, J.K., Scammell, T., Lee, C., Richardson, J.A., Clay Williams, S., Xiong, Y., Kisanuki, Y., et al., 1999. Narcolepsy in orexin knockout mice: Molecular genetics of sleep regulation. Cell 98, 437–451. https://doi.org/10.1016/S0092-8674(00)81973-X

Chew, G.-L., Pauli, A., Rinn, J.L., Regev, A., Schier, A.F., and Valen, E., 2013. Ribosome profiling reveals resemblance between long non-coding RNAs and 5' leaders of coding RNAs. Development 140, 2828–34. https://doi.org/10.1242/dev.098343

Chiu, C.N., Rihel, J., Lee, D.A., Singh, C., Mosser, E.A., Chen, S., Sapin, V., Pham, U., Engle, J., Niles, B.J., et al., 2016. A Zebrafish Genetic Screen Identifies Neuromedin U as a Regulator of Sleep/Wake States. Neuron 89, 842–856. https://doi.org/10.1016/j.neuron.2016.01.007

Cirelli, C., 2009. The genetic and molecular regulation of sleep: from fruit flies to humans. Nat. Rev. Neurosci. 10, 549–60. https://doi.org/10.1038/nrn2683

Cirelli, C., Bushey, D., Hill, S., Huber, R., Kreber, R., Ganetzky, B., and Tononi, G., 2005. Reduced sleep in Drosophila Shaker mutants. Nature 434, 1087–1092. https://doi.org/10.1038/nature03486

Clapcote, S.J., Duffy, S., Xie, G., Kirshenbaum, G., Bechard, A.R., Schack, V.R., Petersen, J., Sinai, L., Saab, B.J., Lerch, J.P., et al., 2009. Mutation I810N in the α3 isoform of Na+,K +-ATPase causes impairments in the sodium pump and hyperexcitability in the CNS. Proc. Natl. Acad. Sci. U. S. A. 106, 14085–14090. https://doi.org/10.1073/pnas.0904817106

Clausen, M. V, Hilbers, F., and Poulsen, H., 2017. The Structure and Function of the Na,K-ATPase Isoforms in Health and Disease. Front. Physiol. 8, 371. https://doi.org/10.3389/fphys.2017.00371

Crambert, G., Fuzesi, M., Garty, H., Karlish, S., and Geering, K., 2002. Phospholemman (FXYD1) associates with Na,K-ATPase and regulates its transport properties. Proc. Natl. Acad. Sci. U. S. A. 99, 11476–81. https://doi.org/10.1073/pnas.182267299

568 Damulewicz, M., Rosato, E., and Pyza, E. (2013). Circadian regulation of the Na+/K+-
569 ATPase alpha subunit in the visual system is mediated by the pacemaker and by retina
570 photoreceptors in Drosophila melanogaster. PLoS One 8, e73690.

571 Dashti, H.S., Jones, S.E., Wood, A.R., Lane, J.M., van Hees, V.T., Wang, H., Rhodes, J.A.,
572 Song, Y., Patel, K., Anderson, S.G., et al. (2019). Genome-wide association study
573 identifies genetic loci for self-reported habitual sleep duration supported by
574 accelerometer-derived estimates. Nat Commun 10, 1100.

575 De Carvalho Aguiar, P., Sweadner, K.J., Penniston, J.T., Zaremba, J., Liu, L., Caton, M.,
576 Linazasoro, G., Borg, M., Tijssen, M.A.J., Bressman, S.B., et al., 2004. Mutations in the
577 Na+/K+-ATPase α3 gene ATP1A3 are associated with rapid-onset dystonia
578 parkinsonism. Neuron 43, 169–175. https://doi.org/10.1016/j.neuron.2004.06.028

579 Despa, S., Tucker, A.L., and Bers, D.M., 2008. Phospholemman-mediated activation of Na/K-
580 ATPase limits [Na]i and inotropic state during β-adrenergic stimulation in mouse
581 ventricular myocytes. Circulation 117, 1849–1855.
582 https://doi.org/10.1161/CIRCULATIONAHA.107.754051

583 Ding, F., O'donnell, J., Xu, Q., Kang, N., Goldman, N., and Nedergaard, M., 2016. Changes
584 in the composition of brain interstitial ions control the sleep-wake cycle. Science (80-.).
585 352, 550–555. https://doi.org/10.1126/science.aad4821

586 Doğanli, C., Beck, H.C., Ribera, A.B., Oxvig, C., and Lykke-Hartmann, K., 2013. α3Na+/K+-
587 ATPase deficiency causes brain ventricle dilation and abrupt embryonic motility in
588 zebrafish. J. Biol. Chem. 288, 8862–8874. https://doi.org/10.1074/jbc.M112.421529

589 Dostanic, I., J. Schultz Jel, J. N. Lorenz, and J. B. Lingrel. 2004. 'The alpha 1 isoform of
590 Na,K-ATPase regulates cardiac contractility and functionally interacts and co-localizes
591 with the Na/Ca exchanger in heart', *J Biol Chem*, 279: 54053-61.Douglas, C.L.,
592 Vyazovskiy, V., Southard, T., Chiu, S.-Y., Messing, A., Tononi, G., and Cirelli, C., 2007.
593 Sleep in Kcna2 knockout mice. BMC Biol. 5, 42. https://doi.org/10.1186/1741-7007-5-42

594 Ewart, H.S., and Klip, A. (1995). Hormonal regulation of the Na(+)-K(+)-ATPase:
595 mechanisms underlying rapid and sustained changes in pump activity. Am J Physiol 269,
596 C295-311.

597 Feschenko, M.S., Donnet, C., Wetzel, R.K., Asinovski, N.K., Jones, L.R., and Sweadner,
598 K.J., 2003. Phospholemman, a single-span membrane protein, is an accessory protein

599 of Na,K-ATPase in cerebellum and choroid plexus. J. Neurosci. 23, 2161–2169.
600 https://doi.org/10.1523/jneurosci.23-06-02161.2003

601 Funato, H., Miyoshi, C., Fujiyama, T., Kanda, T., Sato, M., Wang, Z., Ma, J., Nakane, S.,
602 Tomita, J., Ikkyu, A., et al., 2016. Forward-genetics analysis of sleep in randomly
603 mutagenized mice. Nature 539, 378–383. https://doi.org/10.1038/nature20142

604 Gagnon, J.A., Valen, E., Thyme, S.B., Huang, P., Ahkmetova, L., Pauli, A., Montague, T.G.,
605 Zimmerman, S., Richter, C., and Schier, A.F., 2014. Efficient Mutagenesis by Cas9
606 Protein-Mediated Oligonucleotide Insertion and Large-Scale Assessment of Single-
607 Guide RNAs. PLoS One 9, e98186. https://doi.org/10.1371/journal.pone.0098186

608 Gandhi, A. V, Mosser, E.A., Oikonomou, G., and Prober, D.A., 2015. Melatonin Is Required
609 for the Circadian Regulation of Sleep. Neuron 85, 1–7.
610 https://doi.org/10.1016/j.neuron.2015.02.016

611 Geering, K., Béguin, P., Garty, H., Karlish, S., Füzesi, M., Horisberger, J.D., and Crambert,
612 G., 2003. FXYD proteins: New tissue- and isoform-specific regulators of Na,K-ATPase,
613 in: Annals of the New York Academy of Sciences. New York Academy of Sciences, pp.
614 388–394. https://doi.org/10.1111/j.1749-6632.2003.tb07219.x

615 Giraldez, A.J., Mishima, Y., Rihel, J., Grocock, R.J., Van Dongen, S., Inoue, K., Enright, A.J.,
616 and Schier, A.F., 2006. Zebrafish MiR-430 promotes deadenylation and clearance of
617 maternal mRNAs. Science 312, 75–79. https://doi.org/10.1126/science.1122689

618 Grunwald, H.A., Gantz, V.M., Poplawski, G., Xu, X.R.S., Bier, E., and Cooper, K.L., 2019.
619 Super-Mendelian inheritance mediated by CRISPR–Cas9 in the female mouse germline.
620 Nature. https://doi.org/10.1038/s41586-019-0875-2

621 Heinzen, E.L., Arzimanoglou, A., Brashear, A., Clapcote, S.J., Gurrieri, F., Goldstein, D.B.,
622 Jóhannesson, S.H., Mikati, M.A., Neville, B., Nicole, S., et al., 2014. Distinct neurological
623 disorders with ATP1A3 mutations. Lancet. Neurol. 13, 503–14.
624 https://doi.org/10.1016/S1474-4422(14)70011-0

625 Heinzen, E.L., Swoboda, K.J., Hitomi, Y., Gurrieri, F., De Vries, B., Tiziano, F.D., Fontaine,
626 B., Walley, N.M., Heavin, S., Panagiotakaki, E., et al., 2012. De novo mutations in
627 ATP1A3 cause alternating hemiplegia of childhood. Nat. Genet. 44, 1030–1034.
628 https://doi.org/10.1038/ng.2358

629 Hoffman, E.J., Turner, K.J., Fernandez, J.M., Cifuentes, D., Ghosh, M., Ijaz, S., Jain, R.A.,

630 Kubo, F., Bill, B.R., Baier, H., et al., 2016. Estrogens Suppress a Behavioral Phenotype
631 in Zebrafish Mutants of the Autism Risk Gene, CNTNAP2. Neuron 89, 725–733.
632 https://doi.org/10.1016/j.neuron.2015.12.039

633 Hunanyan, A.S., Fainberg, N.A., Linabarger, M., Arehart, E., Leonard, A.S., Adil, S.M.,
634 Helseth, A.R., Swearingen, A.K., Forbes, S.L., Rodriguiz, R.M., et al., 2015. Knock-in
635 mouse model of alternating hemiplegia of childhood: Behavioral and electrophysiologic
636 characterization. Epilepsia 56, 82–93. https://doi.org/10.1111/epi.12878

637 Iannacone, M.J., Beets, I., Lopes, L.E., Churgin, M.A., Fang-Yen, C., Nelson, M.D., Schoofs,
638 L., and Raizen, D.M., 2017. The RFamide receptor DMSR-1 regulates stress-induced
639 sleep in C. elegans. Elife 6. https://doi.org/10.7554/eLife.19837

640 Ikeda, K., Satake, S., Onaka, T., Sugimoto, H., Takeda, N., Imoto, K., and Kawakami, K.,
641 2013. Enhanced inhibitory neurotransmission in the cerebellar cortex of Atp1a3-deficient
642 heterozygous mice. J. Physiol. 591, 3433–3449.
643 https://doi.org/10.1113/jphysiol.2012.247817

644 Jansen, P.R., Watanabe, K., Stringer, S., Skene, N., Bryois, J., Hammerschlag, A.R., de
645 Leeuw, C.A., Benjamins, J.S., Muñoz-Manchado, A.B., Nagel, M., et al., 2019. Genome-
646 wide analysis of insomnia in 1,331,010 individuals identifies new risk loci and functional
647 pathways. Nat. Genet. 51, 394–403. https://doi.org/10.1038/s41588-018-0333-3

648 Jao, L.-E., Wente, S.R., and Chen, W., 2013. Efficient multiplex biallelic zebrafish genome
649 editing using a CRISPR nuclease system. Proc. Natl. Acad. Sci. U. S. A. 110, 13904–9.
650 https://doi.org/10.1073/pnas.1308335110

651 Johnson, L.S., Eddy, S.R., and Portugaly, E., 2010. Hidden Markov model speed heuristic
652 and iterative HMM search procedure. BMC Bioinformatics 11, 431.
653 https://doi.org/10.1186/1471-2105-11-431

654 Joiner, W.J., 2016. Unraveling the Evolutionary Determinants of Sleep. Curr. Biol. 26,
655 R1073–R1087. https://doi.org/10.1016/j.cub.2016.08.068\

656 Jones, S.E., van Hees, V.T., Mazzotti, D.R., Marques-Vidal, P., Sabia, S., van der Spek, A.,
657 Dashti, H.S., Engmann, J., Kocevska, D., Tyrrell, J., et al. (2019). Genetic studies of
658 accelerometer-based sleep measures yield new insights into human sleep behaviour.
659 Nat Commun 10, 1585.

660 Jumper, J., R. Evans, A. Pritzel, T. Green, M. Figurnov, O. Ronneberger, K.

661 Tunyasuvunakool, R. Bates, A. Zidek, A. Potapenko, A. Bridgland, C. Meyer, S. A. A.
662 Kohl, A. J. Ballard, A. Cowie, B. Romera-Paredes, S. Nikolov, R. Jain, J. Adler, T. Back,
663 S. Petersen, D. Reiman, E. Clancy, M. Zielinski, M. Steinegger, M. Pacholska, T.
664 Berghammer, S. Bodenstein, D. Silver, O. Vinyals, A. W. Senior, K. Kavukcuoglu, P.
665 Kohli, and D. Hassabis. 2021. 'Highly accurate protein structure prediction with
666 AlphaFold', *Nature*, 596: 583-89.

667 Kansagra, S., Ghusayni, R., Kherallah, B., Gunduz, T., McLean, M., Prange, L., Kravitz,
668 R.M., and Mikati, M.A., 2019. Polysomnography findings and sleep disorders in children
669 with alternating hemiplegia of childhood. J. Clin. Sleep Med. 15, 65–70.
670 https://doi.org/10.5664/jcsm.7572

671 Katoh, K., and Toh, H., 2010. Parallelization of the MAFFT multiple sequence alignment
672 program. Bioinformatics. https://doi.org/10.1093/bioinformatics/btq224

673 Kempf, A., Song, S.M., Talbot, C.B., and Miesenböck, G., 2019. A potassium channel β-
674 subunit couples mitochondrial electron transport to sleep. Nature 568, 230–234.
675 https://doi.org/10.1038/s41586-019-1034-5

676 Kimmel, C.B., Ballard, W.W., Kimmel, S.R., Ullmann, B., and Schilling, T.F., 1995. Stages of
677 embryonic development of the zebrafish. Dev. Dyn. 203, 253–310.
678 https://doi.org/10.1002/aja.1002030302

679 Kirshenbaum, G.S., Clapcote, S.J., Duffy, S., Burgess, C.R., Petersen, J., Jarowek, K.J.,
680 Yücel, Y.H., Cortez, M.A., Snead, O.C., Vilsen, B., et al., 2011. Mania-like behavior
681 induced by genetic dysfunction of the neuron-specific Na+,K+-ATPase α3 sodium pump.
682 Proc. Natl. Acad. Sci. U. S. A. 108, 18144–18149.
683 https://doi.org/10.1073/pnas.1108416108

684 Koh, K., Joiner, W.J., Wu, M.N., Yue, Z., Smith, C.J., and Sehgal, A., 2009. Identification of
685 SLEEPLESS, a novel sleep promoting factor. Science (80-.). 321, 372–376.
686 https://doi.org/10.1126/science.1155942.Identification

687 Kristensen, A.S., Andersen, J., Jorgensen, T.N., Sorensen, L., Eriksen, J., Loland, C.J.,
688 Stromgaard, K., and Gether, U., 2011. SLC6 neurotransmitter transporters: Structure,
689 function, and regulation. Pharmacol. Rev. 63, 585–640.
690 https://doi.org/10.1124/pr.108.000869

691 Kwan, K.M., Fujimoto, E., Grabher, C., Mangum, B.D., Hardy, M.E., Campbell, D.S., Parant,

692 J.M., Yost, H.J., Kanki, J.P., and Chien, C.-B., 2007. The Tol2kit: a multisite gateway-
693 based construction kit for Tol2 transposon transgenesis constructs. Dev. Dyn. 236,
694 3088–99. https://doi.org/10.1002/dvdy.21343

695 Lane, J.M., Jones, S.E., Dashti, H.S., Wood, A.R., Aragam, K.G., van Hees, V.T., Strand,
696 L.B., Winsvold, B.S., Wang, H., Bowden, J., et al. (2019). Biological and clinical insights
697 from genetics of insomnia symptoms. Nat Genet 51, 387-393.

698 Lee, D.A., Andreev, A., Truong, T. V., Chen, A., Hill, A.J., Oikonomou, G., Pham, U., Hong,
699 Y.K., Tran, S., Glass, L., et al., 2017. Genetic and neuronal regulation of sleep by
700 neuropeptide VF. Elife 6. https://doi.org/10.7554/eLife.25727

701 Lek, M., Karczewski, K.J., Minikel, E. V., Samocha, K.E., Banks, E., Fennell, T., O'Donnell-
702 Luria, A.H., Ware, J.S., Hill, A.J., Cummings, B.B., et al., 2016. Analysis of protein-
703 coding genetic variation in 60,706 humans. Nature 536, 285–291.
704 https://doi.org/10.1038/nature19057

705 Lenz, O., Xiong, J., Nelson, M.D., Raizen, D.M., and Williams, J.A., 2015. FMRFamide
706 signaling promotes stress-induced sleep in Drosophila. Brain. Behav. Immun. 47, 141–
707 148. https://doi.org/10.1016/j.bbi.2014.12.028

708 Li SB, Damonte VM, Chen C, Wang GX, Kebschull JM, Yamaguchi H, Bian WJ, Purmann C,
709 Pattni R, Urban AE, Mourrain P, Kauer JA, Scherrer G, de Lecea L. Hyperexcitable arousal
710 circuits drive sleep instability during aging. Science. 2022 Feb 25;375(6583):eabh3021.

711 Lin, L., Faraco, J., Li, R., Kadotani, H., Rogers, W., Lin, X., Qiu, X., de Jong, P.J., Nishino, S.,
712 Mignot, E., et al., 1999. The sleep disorder canine narcolepsy is caused by a mutation in
713 the hypocretin (orexin) receptor 2 gene. Cell 98, 365–76. https://doi.org/10.1016/S0092-
714 8674(00)81965-0

715 Love, M.I., Huber, W., and Anders, S., 2014. Moderated estimation of fold change and
716 dispersion for RNA-seq data with DESeq2. Genome Biol. 15, 550.
717 https://doi.org/10.1186/s13059-014-0550-8

718 McGrail, K.M., Phillips, J.M., and Sweadner, K.J., 1991. Immunofluorescent localization of
719 three Na,K-ATPase isozymes in the rat central nervous system: Both neurons and glia
720 can express more than one Na,K-ATPase. J. Neurosci. 11, 381–391.
721 https://doi.org/10.1523/jneurosci.11-02-00381.1991

722 Montague, T.G., Cruz, J.M., Gagnon, J.A., Church, G.M., and Valen, E., 2014. CHOPCHOP:
723 a CRISPR/Cas9 and TALEN web tool for genome editing. Nucleic Acids Res. gku410-.
724 https://doi.org/10.1093/nar/gku410

725 Nakashima, A., Kawamoto, T., Noshiro, M., Ueno, T., Doi, S., Honda, K., Maruhashi, T.,
726 Noma, K., Honma, S., Masaki, T., et al. (2018). Dec1 and CLOCK Regulate Na(+)/K(+)-
727 ATPase beta1 Subunit Expression and Blood Pressure. Hypertension 72, 746-754.

728 Oikonomou, G., Altermatt, M., Zhang, R. wei, Coughlin, G.M., Montz, C., Gradinaru, V., and
729 Prober, D.A., 2019. The Serotonergic Raphe Promote Sleep in Zebrafish and Mice.
730 Neuron 103, 686-701.e8. https://doi.org/10.1016/j.neuron.2019.05.038

731 Palagini, L., Domschke, K., Benedetti, F., Foster, R.G., Wulff, K., and Riemann, D., 2019.
732 Developmental pathways towards mood disorders in adult life: Is there a role for sleep
733 disturbances? J. Affect. Disord. 243, 121–132.
734 https://doi.org/10.1016/J.JAD.2018.09.011

735 Pauli, A., Valen, E., Lin, M.F., Garber, M., Vastenhouw, N.L., Levin, J.Z., Fan, L., Sandelin,
736 A., Rinn, J.L., Regev, A., et al., 2012. Systematic identification of long noncoding RNAs
737 expressed during zebrafish embryogenesis Systematic identification of long noncoding
738 RNAs expressed during zebrafish embryogenesis 577–591.
739 https://doi.org/10.1101/gr.133009.111

740 Pauli, A., Valen, E., and Schier, A.F., 2015. Identifying (non-)coding RNAs and small
741 peptides: Challenges and opportunities. BioEssays 37, 103–112.
742 https://doi.org/10.1002/bies.201400103

743 Pavlovic, D., Fuller, W., and Shattock, M.J., 2013. Novel regulation of cardiac Na pump via
744 phospholemman. J. Mol. Cell. Cardiol. 61, 83–93.
745 https://doi.org/10.1016/j.yjmcc.2013.05.002

746 Peyron, C., Faraco, J., Rogers, W., Ripley, B., Overeem, S., Charnay, Y., Nevsimalova, S.,
747 Aldrich, M., Reynolds, D., Albin, R., et al. (2000). A mutation in a case of early onset
748 narcolepsy and a generalized absence of hypocretin peptides in human narcoleptic
749 brains. Nat Med 6, 991-997.

750 Price, E. M., and J. B. Lingrel. 1988. 'Structure-function relationships in the Na,K-ATPase
751 alpha subunit: site-directed mutagenesis of glutamine-111 to arginine and asparagine-
752 122 to aspartic acid generates a ouabain-resistant enzyme', *Biochemistry*, 27: 8400-8.

753 Prober, D. a, Rihel, J., Onah, A. a, Sung, R.-J., and Schier, A.F., 2006. Hypocretin/orexin
754 overexpression induces an insomnia-like phenotype in zebrafish. J. Neurosci. 26,
755 13400–10. https://doi.org/10.1523/JNEUROSCI.4332-06.2006

756 Reichert, S., Pavón Arocas, O., and Rihel, J., 2019. The Neuropeptide Galanin Is Required
757 for Homeostatic Rebound Sleep following Increased Neuronal Activity. Neuron 104, 370-
758 384.e5. https://doi.org/10.1016/j.neuron.2019.08.010

759 Rihel, J., Prober, D. a, Arvanites, A., Lam, K., Zimmerman, S., Jang, S., Haggarty, S.J.,
760 Kokel, D., Rubin, L.L., Peterson, R.T., et al., 2010. Zebrafish behavioral profiling links
761 drugs to biological targets and rest/wake regulation. Science 327, 348–51.
762 https://doi.org/10.1126/science.1183090

763 Rihel, J., and Schier, A.F., 2013. Sites of action of sleep and wake drugs: insights from model
764 organisms. Curr. Opin. Neurobiol. 23, 831–40.
765 https://doi.org/10.1016/j.conb.2013.04.010

766 Salles, P.A., Mata, I.F., Brunger, T., Lal, D., and Fernandez, H.H. (2021). ATP1A3-Related
767 Disorders: An Ever-Expanding Clinical Spectrum. Front Neurol 12, 637890.

768 Sakurai, T., 2013. Orexin deficiency and narcolepsy. Curr. Opin. Neurobiol. 23, 760–766.
769 https://doi.org/10.1016/j.conb.2013.04.007

770 Sehgal, A., and Mignot, E., 2011. Genetics of sleep and sleep disorders. Cell 146, 194–207.
771 https://doi.org/10.1016/j.cell.2011.07.004

772 Shah, A.N., Davey, C.F., Whitebirch, A.C., Miller, A.C., and Moens, C.B., 2015. Rapid
773 reverse genetic screening using CRISPR in zebrafish. Nat. Methods 12, 535–540.
774 https://doi.org/10.1038/nmeth.3360

775 Shankaran, S.S., Dahlem, T.J., Bisgrove, B.W., Yost, H.J., and Tristani-Firouzi, M., 2017.
776 CRISPR/Cas9-Directed Gene Editing for the Generation of Loss-of-Function Mutants in
777 High-Throughput Zebrafish F $_0$ Screens, in: Current Protocols in Molecular Biology. John
778 Wiley & Sons, Inc., Hoboken, NJ, USA, pp. 31.9.1-31.9.22.
779 https://doi.org/10.1002/cpmb.42

780 Singh, C., Oikonomou, G., and Prober, D.A. (2015). Norepinephrine is required to promote
781 wakefulness and for hypocretin-induced arousal in zebrafish. Elife *4*, e07000.

782 Singh, C., Rihel, J., and Prober, D.A., 2017. Neuropeptide Y Regulates Sleep by Modulating
783 Noradrenergic Signaling. Curr. Biol. 27, 3796-3811.e5.

https://doi.org/10.1016/J.CUB.2017.11.018

Sivasubbu, S., Balciunas, D., Amsterdam, A., and Ekker, S.C., 2007. Insertional mutagenesis strategies in zebrafish. Genome Biol. https://doi.org/10.1186/gb-2007-8-s1-s9

Sugimoto, H., Ikeda, K., and Kawakami, K., 2014. Heterozygous mice deficient in Atp1a3 exhibit motor deficits by chronic restraint stress. Behav. Brain Res. 272, 100–110. https://doi.org/10.1016/j.bbr.2014.06.048

Sweadner, K.J., and Rael, E., 2000. The FXYD gene family of small ion transport regulators or channels: cDNA sequence, protein signature sequence, and expression. Genomics 68, 41–56. https://doi.org/10.1006/geno.2000.6274Therien, A.G., and Blostein, R. (2000). Mechanisms of sodium pump regulation. Am J Physiol Cell Physiol *279*, C541-566.

Thisse, B., Pflumio, S., Fürthauer, M., Loppin, B., Heyer, V., Degrave, A., Woehl, R., Lux, A., Steffan, T., Charbonnier, X.Q. and Thisse, C. (2001) Expression of the zebrafish genome during embryogenesis (NIH R01 RR15402). ZFIN Direct Data Submission. . (http://zfin.org).

Thisse, C., and Thisse, B., 2008. High-resolution in situ hybridization to whole-mount zebrafish embryos. Nat. Protoc. 3, 59–69. https://doi.org/10.1038/nprot.2007.514

Toda, H., Williams, J.A., Gulledge, M., and Sehgal, A., 2019. A sleep-inducing gene, nemuri, links sleep and immune function in Drosophila. Science 363, 509–515. https://doi.org/10.1126/science.aat1650

Ulitsky, I., Shkumatava, A., Jan, C.H., Sive, H., and Bartel, D.P., 2011. Conserved function of lincRNAs in vertebrate embryonic development despite rapid sequence evolution. Cell 147, 1537–1550. https://doi.org/10.1016/j.cell.2011.11.055

Varshney, G.K., Lu, J., Gildea, D.E., Huang, H., Pei, W., Yang, Z., Huang, S.C., Schoenfeld, D., Pho, N.H., Casero, D., et al., 2013. A large-scale zebrafish gene knockout resource for the genome-wide study of gene function. Genome Res. 23, 727–35. https://doi.org/10.1101/gr.151464.112

Villalba, A., Coll, O., and Gebauer, F., 2011. Cytoplasmic polyadenylation and translational control. Curr. Opin. Genet. Dev. 21, 452–457. https://doi.org/10.1016/j.gde.2011.04.006

Wilkinson, R.N., Elworthy, S., Ingham, P.W., and van Eeden, F.J.M., 2013. A method for high-throughput PCR-based genotyping of larval zebrafish tail biopsies. Biotechniques

55, 314–316. https://doi.org/10.2144/000114116

Wittkopp N, Huntzinger E, Weiler C, Saulière J, Schmidt S, Sonawane M, Izaurralde E. Nonsense-mediated mRNA decay effectors are essential for zebrafish embryonic development and survival. Mol Cell Biol. 2009 Jul;29(13):3517-28.

Wu, M., Robinson, J.E., and Joiner, W.J., 2014. SLEEPLESS Is a Bifunctional Regulator of Excitability and Cholinergic Synaptic Transmission. Curr. Biol. 24, 621–629. https://doi.org/10.1016/j.cub.2014.02.026

Wu, R.S., Lam, I.I., Clay, H., Duong, D.N., Deo, R.C., and Coughlin, S.R., 2018. A Rapid Method for Directed Gene Knockout for Screening in G0 Zebrafish. Dev. Cell 46, 112-125.e4. https://doi.org/10.1016/j.devcel.2018.06.003

Zhang, Y., Chen, K., Sloan, S.A., Bennett, M.L., Scholze, A.R., O'Keeffe, S., Phatnani, H.P., Guarnieri, P., Caneda, C., Ruderisch, N., et al., 2014. An RNA-sequencing transcriptome and splicing database of glia, neurons, and vascular cells of the cerebral cortex. J. Neurosci. 34, 11929–11947. https://doi.org/10.1523/JNEUROSCI.1860-14.2014

Materials and Methods

Zebrafish husbandry

All zebrafish lines were housed on a 14hr:10hr light:dark schedule in dechlorinated water at 27.5^{o}C and routine husbandry was performed by the UCL Zebrafish Facility. Embryos were collected from spontaneous spawning and staged according to Kimmel et al. 1995.

Embryos and larvae were raised on a 14hr:10hr light:dark schedule in 10cm Petri dishes at a density of 50 embryos per 10cm Petri dish. Embryo water (~pH7.3, temperature 28.5^{o}C, conductivity ~423.7uS with methylene blue) was changed daily and animals over 4 days post fertilisation were euthanized by overdose of MS-222 (300 mg/l) or 15% 2-Phenoyethanol (77699 SIGMA-ALDRICH) at the end of experiments.

Raising of genetically altered zebrafish and all experimental procedures were performed under project licence 70/7612 and PA8D4D0E5 awarded to JR under the UK Animals (Scientific Procedures) Act 1986 guidelines.

Lines

Strain designation	**Allele Number**	**Gene identifier**	**Additional Information**
10543/dmist^{vir}	*la015577Tg*	ENSDARG00000095754	Maintained at UCL
dmist^{i8}	*u505*	ENSDARG00000095754	Maintained at UCL
fxyd1$^{\Delta 28}$	*u504*	ENSDARG00000099014	Maintained at UCL
atp1a3a$^{\Delta 19}$	*u513*	ENSDARG00000018259	Maintained at UCL
atp1a3b $^{\Delta 14}$	*u514*	ENSDARG00000104139	Maintained at UCL

Table 1. Zebrafish lines

The *dmist^{vir}* allele was generated in wild type line T/AB-5 (Varshney et al., 2013) and outcrossed to Harvard AB. The *dmist^{i8}, fxyd1$^{\Delta 28}$, atp1a3a$^{\Delta 19}$,* and *atp1a3b $^{\Delta 14}$* alleles were generated and maintained at UCL on an AB/TL background. Both *dmist^{i8}* and *dmist^{vir}* were out-crossed to the AB strain at UCL for at least 3 generations.

Larval Zebrafish Behavioural Tracking

At 4 days post fertilisation (dpf), zebrafish larvae were placed into individual wells of a 96-square well plate (WHA7701-1651 Sigma-Aldrich) filled with 650 µl of embryo water per well and tracked for 3 days under a 14:10 light:dark schedule (lights on-09:00, lights off-23:00) using automated videotracking in ViewPoint ZebraBoxes (Viewpoint Life Sciences). The 96-well plate was under constant illumination with infrared LEDs, and white LEDs simulated the light:dark schedule. Videography (with one-third inch Dragonfly2 PointGrey monochrome camera, frame

rate: 25-30 Hz; fixed-angle megapixel lens, Computar M5018-MP) of individual behavior was recorded in quantization mode to detect movement by background subtraction between frames in individual wells with 60 second integration time bins. Parameters used for detection were calibrated according to the sensitivity of individual boxes but were in the following range: detection threshold, 15-20; burst, 50 pixels; freeze, 3-4 pixels. Embryo water in the wells was topped up daily with fresh water, and ambient room temperature was maintained at approximately 26^{o}C. Output data was sorted, parsed and analysed by custom Perl and Matlab scripts (MATLAB R2016 version 9.1, The MathWorks), as in Rihel et al. 2010.

Oxygen-permeable lids (Applied Biosystems 4311971) were applied over the top of the 96-well plate when performing experiments in constant darkness, and the larvae were left undisturbed for the duration of the experiment to avoid light exposure.

At the end of the experiment, all larvae were visually checked for health before euthanasia and transfer to individual wells of a 96-well PCR plate for DNA extraction and genotyping.

Behavioural analysis

Sleep parameters were calculated as in Rihel et al. 2010. For each genotype, exemplar experiments are shown, and summary data was analysed by combining experiments with a linear mixed effects model as follows. Behavioural summaries across multiple experiments were determined by using the Matlab fitlme function to fit a linear mixed effects model for each parameter with genotype as a fixed effect and independent experiment as a random effect, then representing the effect size as a % change from the wild type value. Before fitting the linear mixed effects model, the parameters sleep, sleep length, and waking activity were log normalized by calculating the log of 1+ the parameter value for each larva.

Circadian period for every larva was calculated using the Matlab findpeaks function on the activity (delta-pixels) timeseries data with a minimum peak distance of 18 hours (1080 minutes). N-way ANOVA was calculated to evaluate differences between groups.

Code and data are available at https://github.com/ilbarlow/Dmist.

Adult behavioural tracking

Fish from a *dmist*$^{i8/+}$ x *dmist*$^{i8/+}$ cross were raised in a mixed gender tank to adulthood. Zebrafish adults (aged 3-4 months) were randomly selected and tracked on a 14:10 light:dark cycle (180 lux at water surface, lit from above) for three days as in (Chiu et al., 2016). In brief, fish were placed into uncovered plastic chambers (7x12x8.5 cm; WxLxH) with small holes for water exchange, and these were placed in a circulating water tank (46x54 cm with 4.5 cm water height). This setup was supplied with fish water from the home aquarium heated to 28ºC and pumped from a 45 L reservoir at a flow rate of 1.3 L/min. Infrared light (60 degree, 54 LED Video Camera Red Infrared Illuminator Lamp, SourcingMap, with the ambient light detector covered) was continuously supplied from below. Fish were tracked at 15 Hz using Viewpoint Life Sciences ZebraBox tracking software in tracking mode, with a background threshold of 40, inactive cut-off of 1.3 cm/sec, and a small movement cut-off of 8 cm/sec. Each track was visually inspected for errors at one-minute resolution across the entire session and analysed using custom Matlab scripts (MATLAB R2016 version 9.1, The Mathworks, Inc). Experiments were performed blind to genotype, which was determined by fin-clip after the experiment. Females and males were originally analysed separately; since no significant gender effect was found (two-way ANOVA, genotypeXgender), data from both genders were pooled for the final analysis.

Genotyping

Prior to genotyping, adult fish were anaesthetised in 30 µg/ml MS-222, fin-clipped by cutting a small section of the caudal fin, and then allowed to recover in fresh fish water. For pooled

903 experiments, 3 dpf larvae from heterozygous in-crosses were fin-clipped as in Wilkinson et al.,
904 2013 and allowed to recover in a square 96-well plate to keep larvae separate prior to pooling
905 larvae of the same genotype. Genomic DNA was extracted from adult fin clips and larvae by
906 boiling for 30 minutes in 50 µl 1X base solution (0.025 M KOH, 0.2 mM EDTA). Once cooled,
907 an equal volume (50 µl) of neutralisation buffer (0.04 M Tris-HCl) was then added and undiluted
908 genomic DNA used for genotyping.

909 The *dmist*^{vir} genotype was detected by PCR (standard conditions) using a cocktail of three
910 primers (0.36 mM final concentration each primer) to detect the wild type allele and viral
911 insertion (see Table 2) so that genotypes could be assigned according to size of bands
912 detected (*dmist*$^{vir/vir}$ 800 bp; *dmist*$^{vir/+}$ 508 bp and 800bp; *dmist*$^{+/+}$ 508 bp).

913 The *dmist*^{i8} genotype was assigned by KASP genotyping using allele-specific primers
914 (*dmist*^{i8} allele 5'-GATCTCCCT[GCAGAAAGAT]CTTTCTGCA-3' = FAM, *dmist*$^{+}$ allele 5'-
915 GATCTCCCT[CACCG]CTTTCTGCA-3' = HEX; KASP master mix KBS-1016-011) and assay
916 were prepared and analysed according to manufacturer's protocol (LGC genomics).

917 The *atp1a3a*$^{\Delta 19}$ genotype was assigned by KASP genotyping using allele-specific primers
918 (*atp1a3a*$^{\Delta 19}$ allele 5'-
919 GACAGACTGAAGAAACAGCGACTGACGGCTC[CAAAATGGGGGTAAGAGTC]-3' = FAM,
920 *atp1a3a*$^{+}$ allele 5'-GACAGACTGAAGAAACAGCGACTGACGGCTC-3'[] = HEX).

921 The *atp1a3b*$^{\Delta 14}$ genotype was assigned by PCR using MiSeq_atp1a3b primers (Table 2),
922 with the *atp1a3b*$^{\Delta 14}$ allele running 14 bp faster than the *atp1a3b*$^{+}$ allele.

923 *fxyd1*$^{\Delta 28}$ was assigned by KASP genotyping using allele-specific primers (*fxyd1*$^{\Delta 28}$ allele 5'-
924 GAAGGTCGGAGTCAACGGATTTAATAAACTTTATTGTGCTTTTGTAGTTGT[A]-3' = HEX,
925 *fxyd1*$^{+}$ allele 5'-
926 GAAGGTGACCAAGTTCATGCTTAATAAACTTTATTGTGCTTTTGTAGTTGT[G]-3' = FAM)

or PCR using MiSeq_fxyd1 primers (see Table 2) followed by digestion with the restriction enzyme DrdI, which yields bands at 138 bp and 133 bp for *fxyd1*$^{+/+}$; 138 bp, 133 bp and 271 bp for *fxyd1*$^{+/\Delta 28}$, and 243 bp for *fxyd1*$^{\Delta 28}$.

3'RACE

FirstChoice RLM-RACE kit (Ambion AM1700) was used to amplify the 5' and 3' ends from cDNA obtained from 4 dpf larvae raised on a 14:10 LD cycle and C57BL/6 E13.5 mouse embryos obtained from the Parnavalas lab (UCL). 5' and 3' RACE primers were designed according the manufacturer's guidelines (Table 2) and the manufacturer's protocol was followed. Clones were sequenced by Sanger sequencing.

In situ hybridisation

Probes were designed to target the 3'UTR and entire open reading frame (ORF) of *dmist_Dr* transcript using primers that amplified the target region from zebrafish cDNA under standard PCR conditions (expected size 1325 bp; Table 2). The PCR product was cloned into pSC vector (Strataclone PCR cloning kit Agilent 240205-12) and verified by Sanger sequencing. Antisense probe was generated by cleavage of pSC-dmist plasmid with XbaI and *in vitro* transcribed with T3 polymerase (Promega P2083) using 1 μg DNA template according to the standard *in vitro* transcription protocol (see the full protocol at dx.doi.org/10.17504/protocols.io.ba4pigvn). RNA probe was extracted and purified using the ZYMO RNA concentrator kit (Zymo #R1013).

Whole mount *in situ* hybridisation was performed according to (Thisse and Thisse, 2008) with the following adaptations. Embryos less than 5 dpf were dechorionated and fixed at the appropriate stage in 4% paraformaldehyde (PFA) overnight at 4ºC. 5 dpf larvae were fixed in 4% PFA/4% sucrose overnight at 4ºC and then washed 3x5 min in PBS prior to dissecting out the brain. Fixed embryos were washed 3x5 min in PBS, progressively dehydrated into 100% methanol (MeOH) and stored at -20ºC overnight. Prior to pre-hybridisation embryos were

bleached for 30 min in the dark (0.05% formamide, 0.5X SSC, 6% H_2O_2) and then fixed in 4% PFA for 30 min at room temperature. To image, the embryos were progressively rehydrated into 0.1% PBTw, progressively sunk in to 80% glycerol, and imaged on a Nikon compound microscope (Nikon Eclipse Ni, Leica MC190HD camera).

RT-qPCR

Larvae from heterozygous in-crosses (*dmist*$^{i8/+}$ or *dmist*$^{vir/+}$) were genotyped by tail biopsy at 3 dpf (Wilkinson et al., 2013) and allowed to recover fully in individual wells of a square welled 96-well plate before euthanizing at 5 dpf. RNA was extracted from three 5 dpf embryos of each genotype by snap freezing in liquid nitrogen and TRIzol RNA extraction (Ambion 15596026) with the following modifications to the manufacturer's protocol: 400 µl total TRIzol reagent used to homogenise larvae using a pellet pestle homogenizer, and 5 µg glycogen (Invitrogen Cat No. 10814010; 20 µg/µl) was added to the RNA solution after chloroform extraction to aid precipitation of the RNA. The cDNA library was synthesised from high quality RNA (Agilent AffinityScript qPCR cDNA synthesis kit 600559), diluted 1:10, and gene-specific primers (Table 2) were used for amplification of target genes with SYBR green mastermix in a BioRad CFX Real-Time qPCR instrument. Gene expression levels were normalised to the housekeeping gene *ef1alpha* (primers in Table 2) and analysed using custom Matlab scripts (MATLAB v9.2 2017, The Mathworks 2017).

Sodium Green Assay

Cell permanent Sodium Green tetraacetate (Invitrogen, S6901) was prepared fresh from frozen stock by dissolving in DMSO to 1 mM then diluting in fish water to a final concentration of 10 µM. About 50 larvae (5-7 dpf) from *atp1a3a*$^{\Delta 19/+}$ or dmist$^{i8/+}$ in-crosses were placed in wells of a 6 well plate, then most fish water was removed and replaced with 3 mL of the 10 µM Sodium Green solution for two hours. During exposure, the plate was covered in foil and placed in a 28°C incubator. For PTZ experiments, larvae were also exposed to 10 mM PTZ (diluted

977 from 1 mM stock dissolved in water) for two hours. For timepoints at night (ZT17-19), larvae
978 were handled and collected under red light. After soaking in Sodium Green, larvae were
979 washed 3X with fish water, anaesthetised with MS-2222, and fixed in 4% PFA/4% sucrose
980 overnight at 4°C. After 3X wash in PBS, larval brains were dissected and placed in 200 µL PBS
981 in a 48 well plate, and the matched bodies were used for genotyping (see *Genotyping*). Brains
982 were imaged using an upright MVX10 MacroView microscope with an MC PLAPO 1x objective
983 (both OLYMPUS) with a mercury lamp for fluorescent excitation at 488 nm (OLYMPUS, U-
984 HGLGPS). Images of roughly the same focal plane (dorsal/ventral view) were taken with an XM10
985 OLYMPUS camera by a single exposure following minimal light exposure (to avoid bleaching).
986 Mean fluorescent intensity was calculated from ROIs placed on the optic tectum/midbrain using
987 ImageJ, background subtracted and normalized to the average fluorescence intensity for each
988 imaging session.

989 *Protein Alignments*

990 Cross-species *dmist* homologues were identified by reciprocal BLASTp of the C-terminal
991 region of Dmist_*Dr* in vertebrate genomes. Translations of candidate transcript open reading
992 frames were then aligned with Dmist_*Dr* using ClustalOmega to calculate the percentage
993 identity matrix (www.ebi.ac.uk/Tools/msa/clustalo/) and visualised with the tool Multiple Align
994 Show (www.bioinformatics.org/sms/multi_align.html).

995 To identify Dmist orthologues, Dmist peptides were aligned with the multiple sequence
996 alignment tool MAFFT (Katoh and Toh, 2010) and seeded into a JackHMMR iterative search
997 of the Uniprot database (Johnson et al., 2010). Protein-protein alignments of Dmist to Fxyd1
998 were then performed using ClustalOmega and visualized with the tool Multiple Align Show.

999 *CRISPR/Cas9 gene targeting*

1000 CRISPR targets were designed and synthesised according to Gagnon et al., 2014 using
1001 ChopChop (Montague et al. 2014; http://chopchop.cbu.uib.no/; see Table 2 for sequences) to

identify target sites. 100 pg sgRNA and 300 pg Cas9 mRNA (pT3TS-nCas9n) were injected into the yolk of 1-cell stage AB-TL embryos obtained from natural spawning. F0 fish were screened by high resolution melt (HRM) analysis using gene-specific primers (Table 2) with Precision melt supermix (Biorad 1725112) according to the manufacturer's protocol in a BioRad CFX RT-PCR thermocycler. Positive founders identified in HRM analysis were then sequenced by Illumina MiSeq using gene specific primers with adapters (Table 2) according to the manufacturer's protocol.

Molecular cloning

GFP was fused to the Dmist_*Dr* open reading frame (ORF) by Gateway cloning (Kwan et al., 2007). Gene-specific primers were designed to amplify a PCR product that was recombined with middle donor vector (Table 2; Invitrogen Gateway pDONR221 Cat No. 12536017, Invitrogen Gateway BP Clonase II Cat No. 11789020) to generate a middle entry clone (pME-Dmist). pME-Dmist was recombined with 5' (p5E-CMV/SP6) and 3' (p3E-GFPpA) entry clones and destination vector (pDestTol2pA2) using Gateway Technology (Invitrogen LR Clonase II Plus enzyme Cat No. 12538200) following the manufacturer's protocol.

A 3 bp mutation was introduced into the *CMV:dreammist-GFPpA* by inverse PCR using specific primers (Table 2) and KOD high fidelity hot start polymerase (Millipore 71085). The template was degraded by DpnI digest and circular PCR product was transformed into OneShot TOP10 chemically competent E coli (Invitrogen C4040). Both *CMV:dreammist-GFPpA* and *CMV:dreammistA22W-GFPpA* constructs were checked by Sanger sequencing.

For labelling the plasma membrane, mRNA was *in vitro* transcribed from pCS2-myr-Cherry linearised with NotI, *in vitro* transcribed with SP6 mMessage mMachine (Ambion AM1340), purified and quantified with a QuBit spectrophotometer, and injected at 0.04 μg/μL.

Microinjection and imaging

For Dmist-GFP and DmistA22W-GFP live imaging, embryos from an AB-TL in-cross were injected with 1 nL of plasmid (7 ng/µL). After developing to 90% epiboly, the embryos were placed on a glass coverslip and observed on an inverted confocal microscope (SPinv, Leica) with a 40X objective.

RNAseq

Larvae from heterozygous in-crosses (*dmist*$^{i8/+}$ x *dmist*$^{i8/+}$ and *dmist*$^{vir/+}$ x *dmist*$^{vir/+}$) were raised to adulthood, genotyped and then homozygous mutant and wild type siblings were kept separate. Homozygous mutant and wild-type sibling fish were then in-crossed so that first cousins were directly compared. RNA was extracted from thirty 6 dpf larvae using the same protocol as for RT-qPCR and sent for RNAseq analysis at the UCL Institute of Child Health with a sequencing depth of 75 million reads per sample. Differential analysis of transcript count level between groups was performed as in (Love et al., 2014), and additional analysis was performed using custom Matlab scripts (MATLAB v9.2 2017, The Mathworks 2017).

Mouse RNAseq analysis

The dataset was downloaded from https://web.stanford.edu/group/barres_lab/brain_rnaseq.html; (Zhang et al., 2014) and hierarchical clustering (average linkage) and Pearson correlation calculation analysis were performed using custom Matlab scripts (MATLAB v9.2 2017, The Mathworks 2017).

Experimental Design and Statistical Analyses

Data was tested for normality using the Kolmogorov-Smirnov test. If data were normally distributed, N-way ANOVA (alpha=0.05) was used with correction for multiple comparisons using Tukey's test. If non-parametric, the Kruskal-Wallis test was used with correction for multiple comparisons using Dunn-Sidak (alpha=0.05). Outliers were removed by Grubb's test (threshold $p<0.01$). P values from the linear mixed effects models were determined by are an F-test on the fixed effects coefficients generated from the linear mixed effects model in Matlab.

Data were grouped by genotype and gender for adult experiments and grouped by genotype and day of experiment for larval experiments.

All code is available at https://github.com/ilbarlow/Dmist.

Table 2. Primer Sequences

	Oligo Name	Sequence (5' -> 3')	Annealing temperature (oC)	Application
1	dmist_vir_fw	CACAGGGATGTGATGCCGGTTAAC	55	dmistvir genotyping
2	dmist_vir_rev	GTAGACACATACTGCCATACCAATC	55	dmistvir genotyping
3	vir_fw	CACCAGCTGAAGCCTATAGAGTACGAGC-	55	dmistvir genotyping
4	dmist_Dr_5RACE_fw	CGTTTCGCCACAATGTCAGCA	55-65	dmist_Dr 5'RACE
5	dmist_Dr_5RACE_rev_outer	AATGTTCAACTCCAGGCGTC	55-65	dmist_Dr 5'RACE
6	dmist_Dr_5RACE_rev_inner	AATGTTCAACTCCAGGCGTC	55-65	dmist_Dr 5'RACE
7	dmist_Dr_3RACE_fw_inner	GACGCCTGGAGTTGAACATT	55-65	dmist_Dr 3'RACE
8	dmist_Dr_3RACE_fw_outer	GGTATGGCAGTATGTGTCTACA	55-65	dmist_Dr 3'RACE
9	Dmist_Mm_3RACE_outer	GCTGGTGACTGTCCTCCTTATG	55-65	dmist_Mm 3'RACE
10	Dmist_Mm_3RACE_inner	GTGTCTACAAGCCCATCCGTC	55-65	dmist_Mm 3'RACE
11	dmist_Dr_fw	TTTCGCCACAATGTCAGCAGC	56	dmist_Dr probe
12	dmist_Dr_rev	CGACTTTCATTTATTAGTTCAGACATGTC	56	dmist_Dr probe
13	qPCR_dmist_fw	ACGCCAGACCTTATGAAATCC	60	RT-qPCR
14	qPCR_dmist_rev	TGCGTCGGAGAGGTTTGTAG	60	RT-qPCR
15	qPCR_ankrd13a_fw	TGGTGGCGTTCCAGAGTTAC	60	RT-qPCR
16	qPCR_ankrd13a_rev	GGACACGAGAGGAATCCAGC	60	RT-qPCR
17	qPCR_slc6a4b_fw	ACATGGTTGGGTCGACGTTT	60	RT-qPCR
18	qPCR_slc6a4b_rev	TCCAACCCACCAAAAGTGCT	60	RT-qPCR
19	ef1alpha_fw	TGCTGTGCGTGACATGAGGCAG	60	RT-qPCR
20	ef1alpha_rev	CCGCAACCTTTGGAACGGTGT	60	RT-qPCR
21	SP6dmist_sgRNA	ATTTAGGTGACACTATAGCGTTATGCAGAAAGCGGTGGTTTTAGAGCTAGAAATAGCAAG	n/a	CRISPR
22	T7atp1a3a_sgRNA	TAATACGACTCACTATAGACTGACGGCTCCAAAATGGGTTTTAGAGCTAGAAATAGCAAG	n/a	CRISPR
23	SP6fxyd1_sgRNA	ATTTAGGTGACACTATAGGACCCTCTGCCAACACAAGGTTTTAGAGCTAGAAATAGCAAG	n/a	CRISPR
24	SP6atp1a3b_sgRNA	ATTTAGGTGACACTATAGGACTGACTGCGCAACCATGGTTTTAGAGCTAGAAATAGCAAG	n/a	CRISPR
25	HRM_dmist_fw	GCCACAATGTCAGCAGCACG	59	HRM
26	HRM_dmist_rev	GCGTTCACTTTAGACTCTCCCAGC	59	HRM
27	HRM_atp1a3a_fw	TGACAGACTGAAGAAACAGC	55	HRM
28	HRM_atp1a3a_rev	TTAAATCTCAGCACCAGCAG5	55	HRM
29	HRM_fxyd1_fw	TGACCAAACCTTCTTAAGGTGC	58	HRM
30	HRM_fxyd1_rev	AAATTGAGAAGACTTACTGGTCTGC	58	HRM
31	HRM_atp1a3b_fw	AAAGGCTGTCACTTTCTCCATCAC5	58	HRM
32	HRM_atp1a3b_rev	TGCAGTAGATGAGGAATCGGTC	58	HRM
33	MiSeq_dmist_fw	TCGTCGGCAGCGTCAGATGTGTATAAGAGACAGTATAACTTACGTGTGGACGGACTC	58	MiSeq
34	MiSeq_dmist_rev	GTCTCGTGGGCTCGGAGATGTGTATAAGAGACAGTTGCCTCAGCAGGATTTCATAAG	58	MiSeq
35	MiSeq_atp1a3a_fw	TCGTCGGCAGCGTCAGATGTGTATAAGAGACAGTCGTTATCCGTGCAAGAGCTTC	58	MiSeq
36	MiSeq_atp1a3a_rev	GTCTCGTGGGCTCGGAGATGTGTATAAGAGACAGTTCTCAGCACCAGCAGTTATCG	58	MiSeq
37	MiSeq_atp1a3b_fw	TCGTCGGCAGCGTCAGATGTGTATAAGAGACAGTGACTGACATTCTCTCTTCGTG	68	MiSeq
38	MiSeq_atp1a3b_rev	GTCTCGTGGGCTCGGAGATGTGTATAAGAGACAGTTCTCTGTGATGCAGTAGATGAGG	68	MiSeq
39	MiSeq_fxyd1_fw	TCGTCGGCAGCGTCAGATGTGTATAAGAGACAGAAATACTGTCTTGTGACCAAACC	57	MiSeq
40	MiSeq_fxyd1_rev	GTCTCGTGGGCTCGGAGATGTGTATAAGAGACAGTTCATCCTCTGCTGCAAAATGC	57	MiSeq
41	attB1-dreammist forward primer	GGGGACAAGTTTGTACAAAAAAGCAGGCTTCACCATGTCAGCAGCACGCCTGATCTCC	55-60	Gateway
42	attB3-dreammist reverse primer	GGGGACCACTTTGTACAAGAAAGCTGGGTATCACCTGCGTCGGAGAGGTTTGTAG	55-60	Gateway
43	Dmist-GFPA22WFw	GCTTTTCCAGTCTGGGAGT**TGG**CAGCTGGGAGAGTCTAAAG	66	SDM
44	Dmist-GFPA22WRev	CTTTAGACTCTCCCAGCTG**CCA**ACTCCCAGACTGGAAAAGC	66	SDM

FIGURE LEGENDS

Figure 1. A viral insertion mini-screen identifies a short-sleeping mutant, *dreammist.*

A-B) Mean± SEM sleep (A) and waking activity (B) of progeny from *dmist*$^{vir/+}$ in-cross from original screen. White blocks show day (lights on) and grey blocks show night (lights off). Data is combined from 2 independent experiments. n indicates the number of animals.

C-F) Analysis of sleep/wake architecture for the data shown in (A, B). C) Quantification of total sleep across two days and nights shows decreased day and night sleep in *dmist*$^{vir/vir}$. Analysis of sleep architecture reveals fewer sleep bouts during the day (D) and shorter sleep bouts at night (E) in *dmist*$^{vir/vir}$ compared with sibling controls. F) Daytime waking activity is also increased in *dmist*$^{vir/vir}$. The black lines show the mean ± SEM, except in E, which labels the median ± SEM. *p<0.05, **p<0.01, ***p<0.001; ns p>0.05; one-way ANOVA, Tukey's post hoc test.

G) Combining 5 independent experiments using a linear mixed effects model with genotype as a fixed effect and experiment as a random effect reveals *dmist*$^{vir/vir}$ larvae have decreased total sleep and changes to sleep architecture during both the day and night compared to *dmist*$^{+/+}$ siblings. Plotted are the genotype effect sizes (95% confidence interval) for each parameter relative to wild type. Shading indicates day (white) and night (grey). P-values are assigned by an F-test on the fixed effects coefficients from the linear mixed effects model. *p<0.05, **p<0.01, ***p<0.001, ns p>0.05. n indicates the number of animals.

Figure 2. *dmist* encodes a conserved vertebrate single pass transmembrane protein.

A) *dmist* mutants harbour a viral insertion in the 1st intron of *si:key-234h16.7*. *dmist* is syntenic with *Ankrd13* and *GIT* orthologs in mouse, human, and zebrafish.

B) RT-qPCR of *dmist* (red) show reduced expression of *dmist* and not the 5' and 3' flanking zebrafish genes, *slc6a4b* (cyan) and *ankrd13a* (blue), in *dmist*$^{vir/vir}$ larvae compared to *dmist*$^{vir/+}$ and *dmist*$^{+/+}$ siblings. **p<0.01, *p<0.05; ns p>0.05; one-way ANOVA, Tukey's post-hoc test. Data shows mean ± SEM normalized to the wild type mean.

C) *dmist_Dr* contains an open reading frame encoding a 70 amino acid protein that is conserved across vertebrates. All identified homologues have a predicted signal peptide sequence (magenta line), signal peptide cleavage site (magenta circle), and predicted transmembrane domain (grey), with additional highly conserved C-terminal motifs (blue lines). Identical amino acids in all species are shown in black; similar amino acids (80-99% conserved across species) are shown in grey.

D) *In situ* hybridisation using a *dmist* antisense probe reveals *dmist* is maternally deposited as it is detected at the 2-cell stage. At 24 hpf expression is restricted to regions containing neuronal precursors, and at 5 dpf expression is widespread throughout the brain. Tel, telencephalon; Dien, diencephalon; R1-6, rhombomeres 1-6; A, anterior; P, posterior. Scale bars= 0.5 mm (2 cell and 24 hpf), 0.1 mm (5 dpf).

E-F) Representative confocal image of 90% epiboly embryo co-injected at the 1-cell stage with mRNA encoding membrane-RFP (magenta) and a plasmid encoding either C-terminal tagged Dmist-GFP (E, green) or DmistA22W-GFP (F, green). Scale bar= 25 μm.

Figure 3. CRISPR-generated *dmist* mutants sleep less and are hyperactive at night.

A) CRISPR/Cas9 targeting of the first exon of *dmist* resulted in an 8 bp insertion (*dmist*^{i8}) (grey line) within the coding sequence, leading to an early stop codon (red line with *). Guide RNA target sequence and PAM sequence are shown as black bars. The sequence that is deleted in the mutant is indicated with a red bar.

B) Predicted Dmist^{i8} peptide sequence lacks most of the N-terminal signal peptide sequence (magenta) and the full C-terminus.

C-D) Representative 48 hr traces of mean ± SEM sleep (C) and waking activity (D) shows decreased sleep and increased waking activity at night for *dmist*$^{i8/i8}$ fish compared to *dmist*$^{i8/+}$ and *dmist*$^{+/+}$ siblings. n=number of fish.

E-H) Analysis of sleep/wake architecture of the experiment depicted in (C, D) indicates that *dmist*$^{i8/i8}$ larvae sleep less at night (E) due to fewer sleep bouts (F). Sleep bout length is unchanged (G). Waking activity is also increased in *dmist*$^{i8/i8}$ fish (H). The black line represents the mean ± SEM except for G, which is the median ± SEM. *p<0.05, **p<0.01, ***p<0.001; One-way ANOVA, Tukey's post hoc test.

I) Combining 5 independent experiments with a linear mixed effects model reveals *dmist*$^{i8/i8}$ fish sleep less at night due to fewer sleep bouts and also show increased waking activity at night. Plotted are the genotype effect sizes (95% confidence interval) for each parameter relative to wild type. Shading indicates day (white) and night (grey). P-values are assigned by an F-test on the fixed effects coefficients from the linear mixed effects model. *p<0.05, **p<0.01, ***p<0.001, ns p>0.05.

J-K) (J) Adult *dmist*$^{i8/i8}$ fish have a higher mean swim speed compared to their wild type siblings at night. Data in (J) is quantified at night in (K). (J, K) show mean ± SEM. *p<0.05, one-way ANOVA.

L) Cumulative probability distribution of all night-time swim bout speeds in adult fish. The dashed lines show the half max (0.5 probability) for each curve. *p<0.05 for *dmist*$^{i8/i8}$ fish compared to wild type siblings; Kolmogorov-Smirnov test.

Figure 4. Mutation of the *dmist* related gene *fxyd1* causes reduced sleep at night.

A) Schematic of zebrafish Dmist and Fxyd1 protein domains and alignments comparing human, mouse, and zebrafish Dmist and FXYD1 protein sequences. Black and grey shading indicate amino acid identity and similarity, respectively. The FXYD domain is indicated with a red line and the RRR motif in the C-terminus is indicated with a dark blue line.

B) CRISPR-Cas9 targeting of the 3rd exon of *fxyd1* created a 28 bp deletion, resulting in a predicted truncated protein. The start codon is marked by a cyan line. Guide RNA target sequence and PAM sequence are shown as black bars. The mutant deleted sequence is indicated with a red bar.

C) *In situ* hybridisation of *fxyd1* at 24 hpf (whole animal) and 5 dpf brain (ventral view). Anterior is to the left. Scale bar = 0.5 mm (24 hpf); 0.1 mm (5 dpf).

D-E) Representative behavioral experiment showing *fxyd1*$^{\Delta 28}$ mutants have decreased night-time sleep (D) but normal waking activity at night (E).

F) Combining 5 independent experiments with a linear mixed effects model reveals *fxyd1*$^{\Delta 28/\Delta 28}$ larvae sleep significantly less at night due to shorter sleep bouts compared to *fxyd1*$^{+/+}$ siblings. Plotted are the genotype effect sizes (95% confidence interval) on each parameter relative to wild type. Shading indicates day (white) and night (grey). P-values are assigned by an F-test on the fixed effects coefficients from the linear mixed effects model. *p<0.05, **p<0.01, ***p<0.001, ns p>0.05.

Figure 5. Mutation of the Na^+/K^+ pump alpha subunit *atp1a3a* reduces sleep at night

A-B) Mean ± SEM sleep and waking activity traces of wild type larvae following exposure to 1 µM ouabain. Arrows indicate time the drug was added.

C-D) At night, sleep is significantly reduced and waking activity is significantly increased after ouabain exposure. Student's t-test, one tailed.

E) Alignments of Na^+/K^+ pump alpha subunits around the ouabain binding sites. Red indicates residues that are critical for higher sensitivity to ouabain, which are present in mouse Atp1a3 but not Atp1a1.

F) *In situ* hybridisation of *atp1a3a* at 24hpf (whole animal) and 5dpf brain (ventral view). Anterior is to the left. Scale bar = 0.5 mm (24 hpf); 0.1 mm (5 dpf). A-anterior; P-posterior; D-Dorsal; V-Ventral

G) CRISPR-Cas9 targeting of the *atp1a3a* resulted in a 19 bp deletion that eliminates the start codon (blue) and splice junction. Guide RNA target sequence and PAM sequence are shown as black bars. Sequence that is deleted in the mutant is indicated with a red bar.

H-I) Representative behavioural experiment showing *atp1a3a*$^{\Delta 19/\Delta 19}$ fish are hyperactive throughout the day-night cycle and have decreased sleep at night. Mean ± SEM are shown.

J) *atp1a3a*$^{\Delta 19/\Delta 19}$ larvae sleep less at night due to shorter sleep bouts. Plotted are the genotype effect sizes (95% confidence interval) on each parameter relative to wild type. Shading indicates day (white) and night (grey). P-values are assigned by an F-test on the fixed effects coefficients from the linear mixed effects model. *p<0.05, **p<0.01, ***p<0.001, ns p>0.05.

Figure 6. *dmist* mutants have altered sodium homeostasis

A) Brain sodium levels are significantly elevated after exposure to PTZ in both *atp1a3a*$^{\Delta 19/\Delta 19}$ (2 independent experiments) and *dmist*$^{i8/i8}$ (4 independent experiments) fish relative to wild type and heterozygous mutant siblings, as measured by fluorescence intensity of Sodium Green, normalized to the sample mean intensity. Crosses show mean ± SEM. n indicated the number of animals. Below are example images of brains stained with Sodium Green. *p<0.05, **p<0.01, one-way ANOVA, Tukey's post hoc test.

B) Under baseline conditions, brain sodium levels are significantly elevated in *dmist*$^{i8/i8}$ fish at night but not during the day, as measured by fluorescence intensity with Sodium Green. Crosses show mean ± SEM. *p<0.05, **p<0.01, one-way ANOVA, Tukey's post hoc test.

C) *dmist*$^{i8/i8}$ larvae have increased rebound sleep compared to wild type siblings following exposure to 5mM PTZ. Representative sleep traces of *dmist*$^{+/+}$ (no drug, water vehicle controls in black; PTZ exposed in blue) and *dmist*$^{i8/i8}$ (no drug in purple; PTZ exposed in red) following 1 hr exposure to 5 mM PTZ (black bar) in the morning. Data are mean ± SEM. *dmist*$^{i8/+}$ animals are not plotted for clarity but are included in panel D.

D) Rebound sleep after exposure to 5 mM PTZ, calculated from the experiment in C. Each dot represents a single fish, grey lines show mean ± SEM.

E) Effect size of change in sleep after 1 hr treatment with 5 mM PTZ (and washout) compared to vehicle treated controls (error bars show 95% confidence intervals). *p<0.05, one-way ANOVA, Tukey's post-hoc test.

F) Effect sizes (and 95% confidence interval) relative to wild types (dotted line) on sleep at night in larvae from *dmist*$^{+/-}$; *atp1a3a*$^{+/-}$ in-crosses from 3 independent experiments. P-values are assigned by an F-test on the fixed effects coefficients from the linear mixed effects model relative to *dmist*$^{+/+}$; *atp1a3a*$^{+/+}$ animals. For all sleep-wake parameters, see Figure S6. *p<0.05, **p<0.01, ***p<0.0001, ns p>0.05.

Figure S1. A viral insertion screen for sleep-wake regulators

A) Schematic of screening strategy. Candidate genes were selected from a list of 904 mammalian genes encoding protein classes most often linked to behavioural regulation, including 1) genes previously implicated in sleep and circadian rhythms; 2) G-protein coupled receptors; 3) neuropeptide ligands; 4) channels; and 5) proteins involved in post-translational regulation, such as de-ubiquitinating enzymes (Supplemental Data 1). tBLASTN of the human protein sequences identified 1162 zebrafish orthologs (Zv6), of which 702 (60.4%) had viral insertions mapped in the 'Zenemark' zebrafish viral insertion library (Varshney et al., 2013). Sperm harbouring viral insertions in 26 loci were successfully used for *in vitro* fertilization and propagated to the F3 generation for screening. F3 larvae from single family F2 in-crosses were monitored on a 14hr:10hr light:dark cycle from 4-7 dpf using videography and genotyped at the end of the experiment.

B-C) Histogram of total daytime sleep (B) and average daytime waking activity (C) normalized as standard deviations from the mean (Z-score) of all the viral-insertion lines tested (including heterozygous *vir/+* and homozygous *vir/vir*). Line 10543 (renamed *dreammist*) exhibited decreased daytime sleep and increased daytime waking activity.

Figure S2. *dmist*$^{vir/vir}$ fish are hyperactive and have normal circadian rhythms.

A) Free-running circadian period length of the locomotor activity of larvae from a *dmist*$^{vir/+}$ in-cross following the transition at 5 dpf from a 14hr:10hr light:dark cycle to constant dark conditions. The data is quantified for 48 hours after the shift to darkness and shows no difference in period between *dmist*$^{vir/vir}$ larvae and their sibling controls. Data is from 3 independent experiments. $p>0.05$, one-way ANOVA, Tukey's post hoc test.

B-C) Representative mean ± SEM sleep (B) and waking activity (C) traces of animals used to calculate circadian period length in (A). Light and dark grey blocks show subjective day and night, respectively.

D) RT-qPCR time-course before (light) and after (grey) transfer into constant dark demonstrates that *dmist* mRNA levels do not oscillate with a circadian period, unlike *per1* mRNA which does. n=3 replicates per timepoint. Expression is normalized to circadian time 3. Data are mean ± SEM.

Figure S3. *dmist* is enriched in neurons and requires the signal peptide cleavage site for membrane localisation.

A) Relative expression level of *dmist* transcript from RNA sequencing of 6 dpf *dmist*$^{vir/vir}$ and *dmist*$^{+/+}$ siblings. Z-scores were calculated by subtracting mean expression and normalising by the standard deviation across all expressed transcripts (27,243 transcripts). Data show mean ± SEM from 3 independent biological replicates. **p<0.01 Student's t-test.

B) 3' and 5' RACE identify a long (1100 bp) and short (215 bp) 3'UTR variant in *dmist_Dr*, and a long 3'UTR (1050 bp) in *Dmist_Mm*. The purple arrow indicates the ISH probe used in Figure 2D.

C) *dmist_Dr* sense probe negative control at 24 hpf shows no detectable expression.

D) Percentage identity matrix comparing *Dmist* homologues across 6 vertebrate species (100%=magenta; >70%=purple; >50%=cyan; <50%=green).

E) Hierarchical clustering of RNAseq dataset of 6 different cell types isolated from the developing (E13.5) mouse brain (Zhang et al., 2014) and post-hoc identification of *Dmist_Mm*. Data was standardized by subtracting the mean expression and normalizing by the standard deviation across all expressed transcripts in each cell type (column). *Dmist_Mm* (green arrow) co-clusters with genes highly expressed in neurons (green shaded branches).

F) Pearson rank correlation of canonical cell-type markers with *Dmist_Mm* shows high co-expression with neuronal markers compared to astroglial and endothelial cell markers. Data are mean ± SEM. *p<0.05, **p<0.01; Kruskal-Wallis, Dunn-Sidak post-hoc test.

G-I) Predicted processing of Dmist to its mature form in the plasma membrane (G). C-terminal GFP fusion to Dmist is predicted to localise to the membrane (H). However, a mutation (A22W) at the signal peptide cleavage site (I) is predicted to inhibit signal peptide cleavage and so prevent proper subcellular localisation of the mature protein.

Figure S4. CRISPR-generated *dmist* mutants have reduced *dmist* transcript levels

A) RT-qPCR shows *dmist*$^{i8/i8}$ larvae have reduced *dmist* mRNA levels, suggesting that *dmist*^{i8} transcripts undergo nonsense mediated decay. Data are mean ± SEM of three biological replicates. **p<0.01; one-way ANOVA, Tukey's post-hoc test.

B) Relative expression level of *dmist* transcript from RNA sequencing of 6 dpf *dmist*$^{i8/i8}$ and *dmist*$^{+/+}$ siblings. Z-score calculated by subtracting mean expression and normalising by the standard deviation across all expressed transcripts. Data are mean ± SEM for 3 independent biological replicates. **p<0.01, Student's t-test.

Figure S5. Ouabain dose curve and effects of *atp1a3b* mutation on behaviour.

A) Dose response curve of ouabain's effects on sleep at night, shown as mean ± SEM and normalized to the DMSO control. Each data point represents a single fish.

B) Pearson rank correlation of canonical cell-type markers with *Atp1a3a_Mm* shows high co-expression with neuronal markers compared to astroglial and endothelial cell markers. Data are mean ± SEM.

C) *In situ* hybridisation of *atp1a3a* at 24 hpf (whole animal) and 5 dpf brain (ventral view). Anterior is to the left. Scale bar = 0.5 mm (24 hpf); 0.1 mm (5 dpf).

D) CRISPR-Cas9 targeting of *atp1a3b* resulted in a 14 bp deletion that eliminates the start codon (blue). Guide RNA target sequence and PAM sequence are shown as black bars. The sequence that is deleted in the mutant is indicated with a red bar.

E-F) Representative single behavioural experiment showing *atp1a3b*$^{\Delta 14/\Delta 14}$ mutants have increased daytime waking activity but normal sleep patterns.

G) Data from 2 independent experiments combined with a linear mixed effects model. Plotted are the genotype effect sizes (95% confidence interval) for each parameter relative to wild type (dotted line) for each genotype. Shading indicates day (white) and night (grey). n indicates the number of animals. P-values are assigned by an F-test on the fixed effects coefficients from the linear mixed effects model relative to *atp1a3b*$^{+/+}$ animals. *p<0.05.

Figure S6. Sleep effects in *dmist*$^{-/-}$; *atp1a3a*$^{-/-}$ double mutants are non-additive.

Combining 3 independent experiments with a linear mixed effects model reveals that the effects of loss of function *dmist* and *atp1a3a* mutations are non-additive. Plotted are the genotype effect sizes (95% confidence interval) for each parameter relative to wild type for each genotype. Shading indicates day (white) and night (grey). n indicates the number of animals.

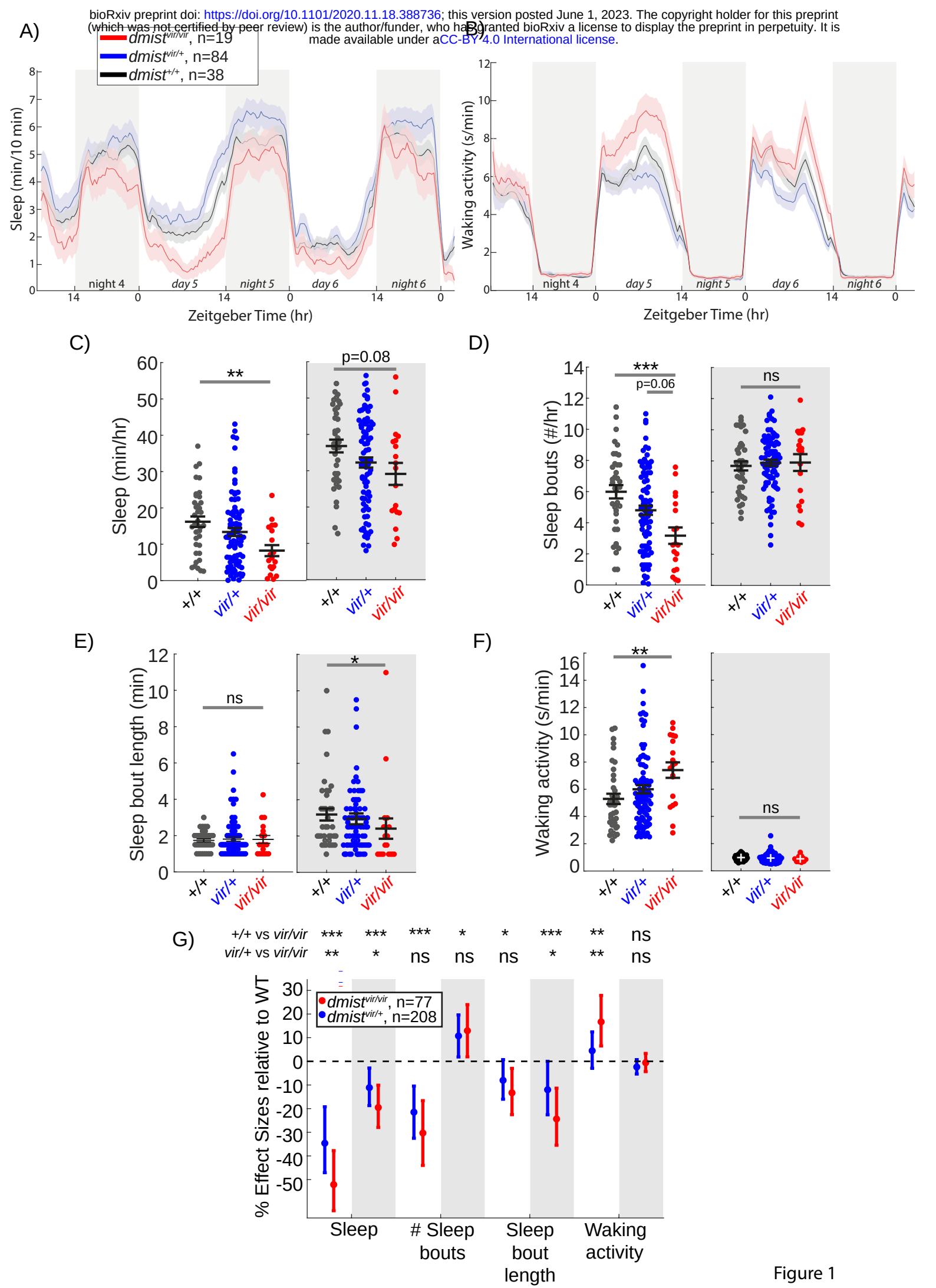

Figure 1

A)

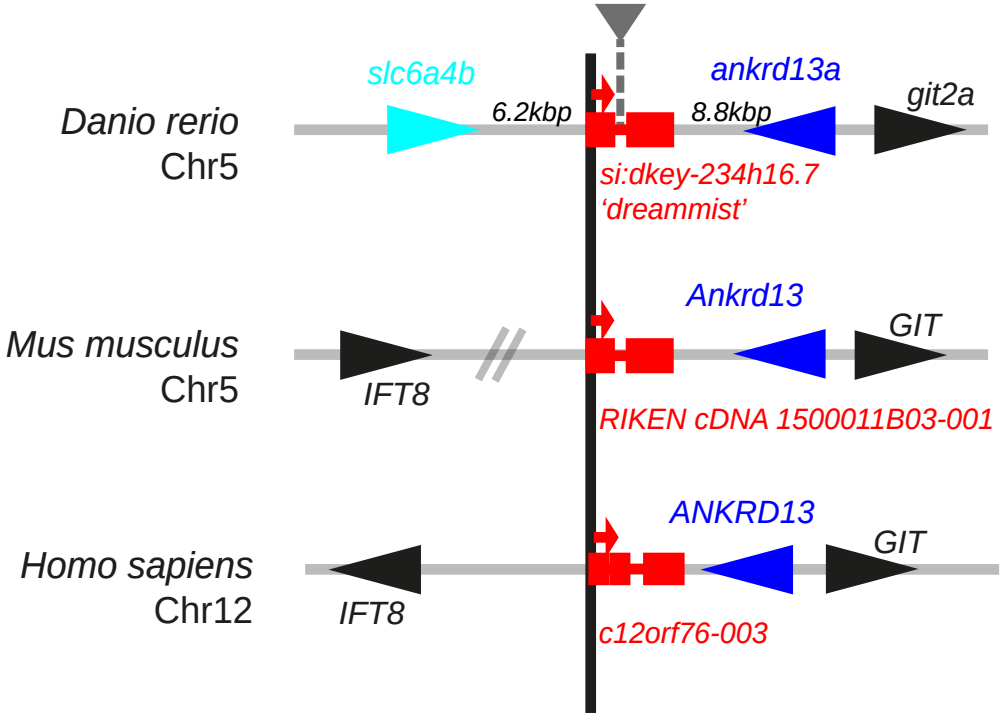

B)

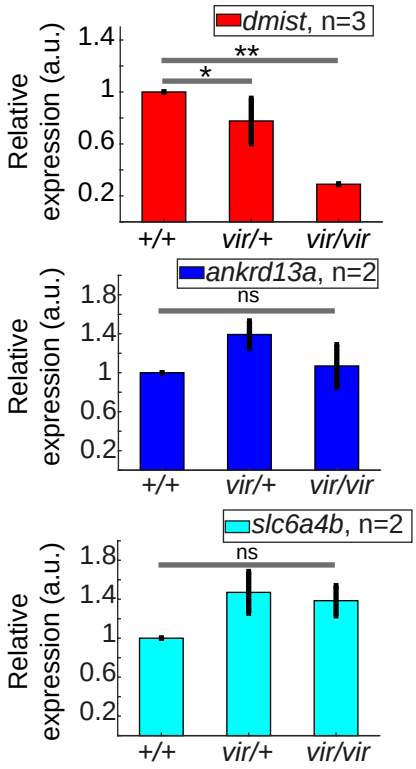

C)

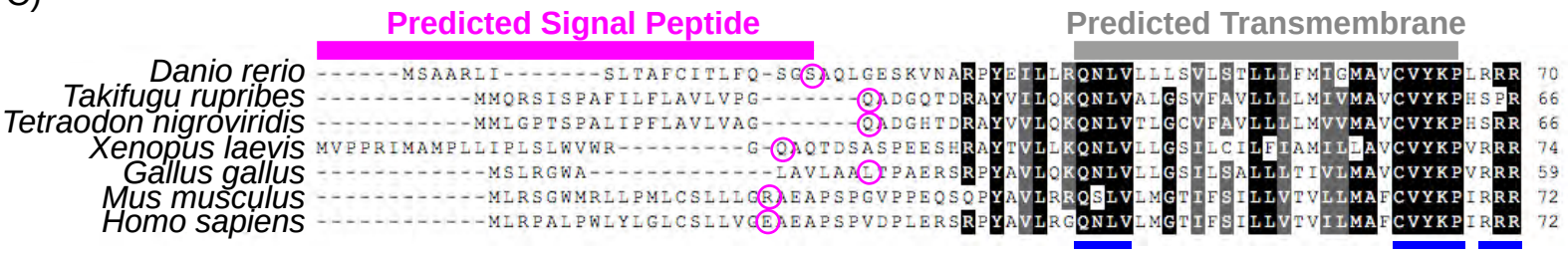

D)

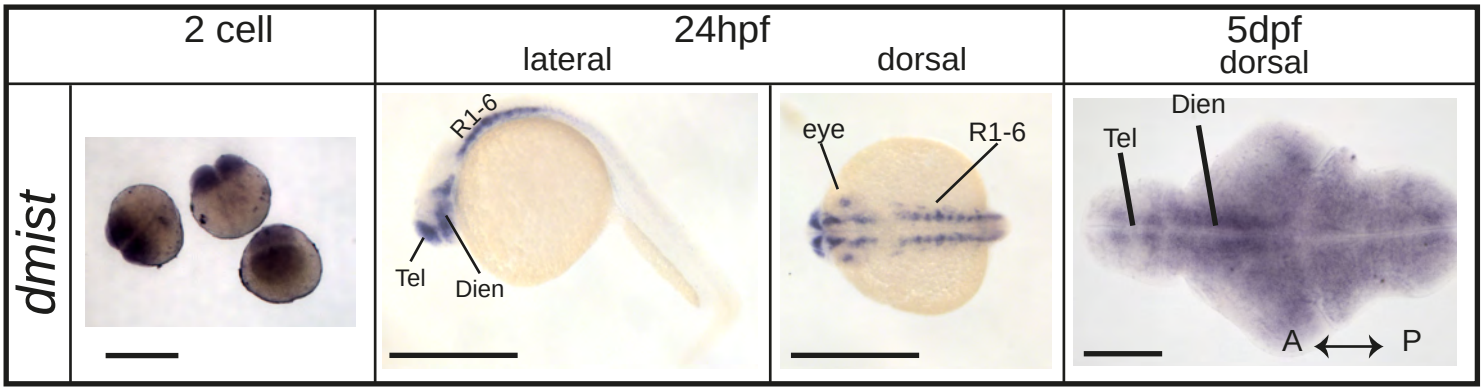

E)

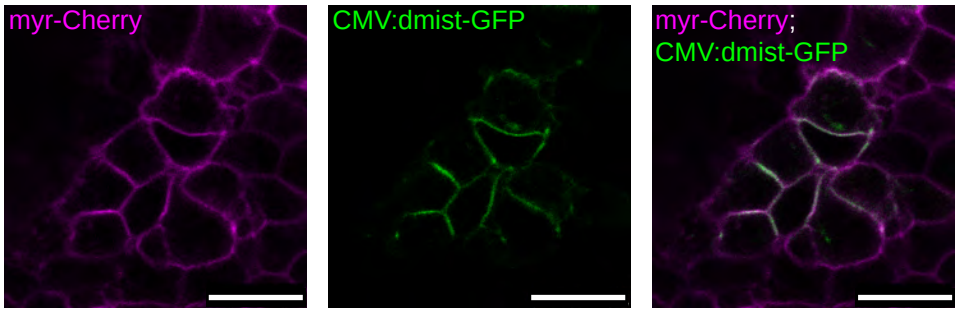

F)

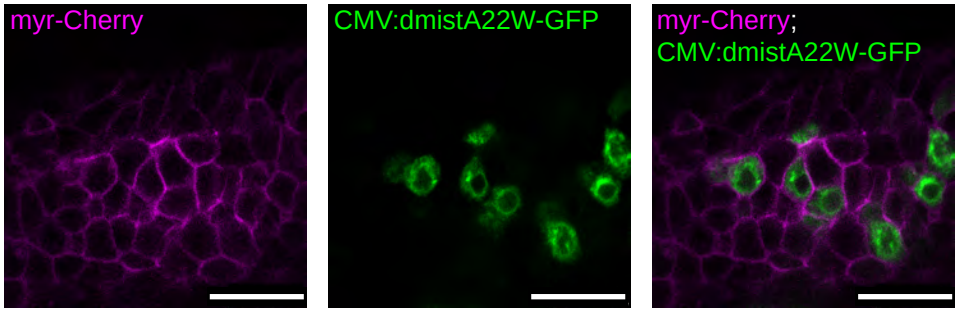

Figure 2

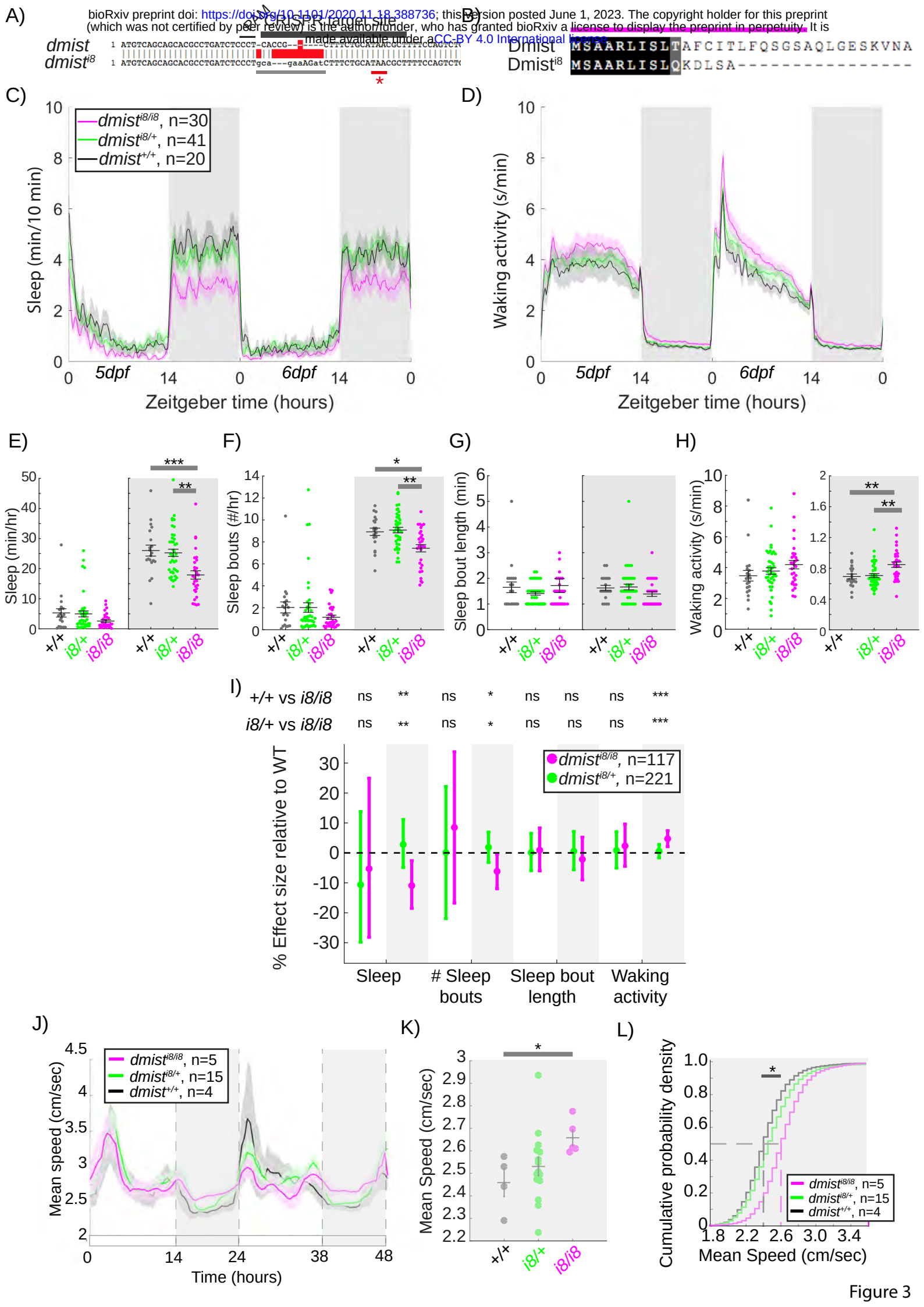

Figure 3

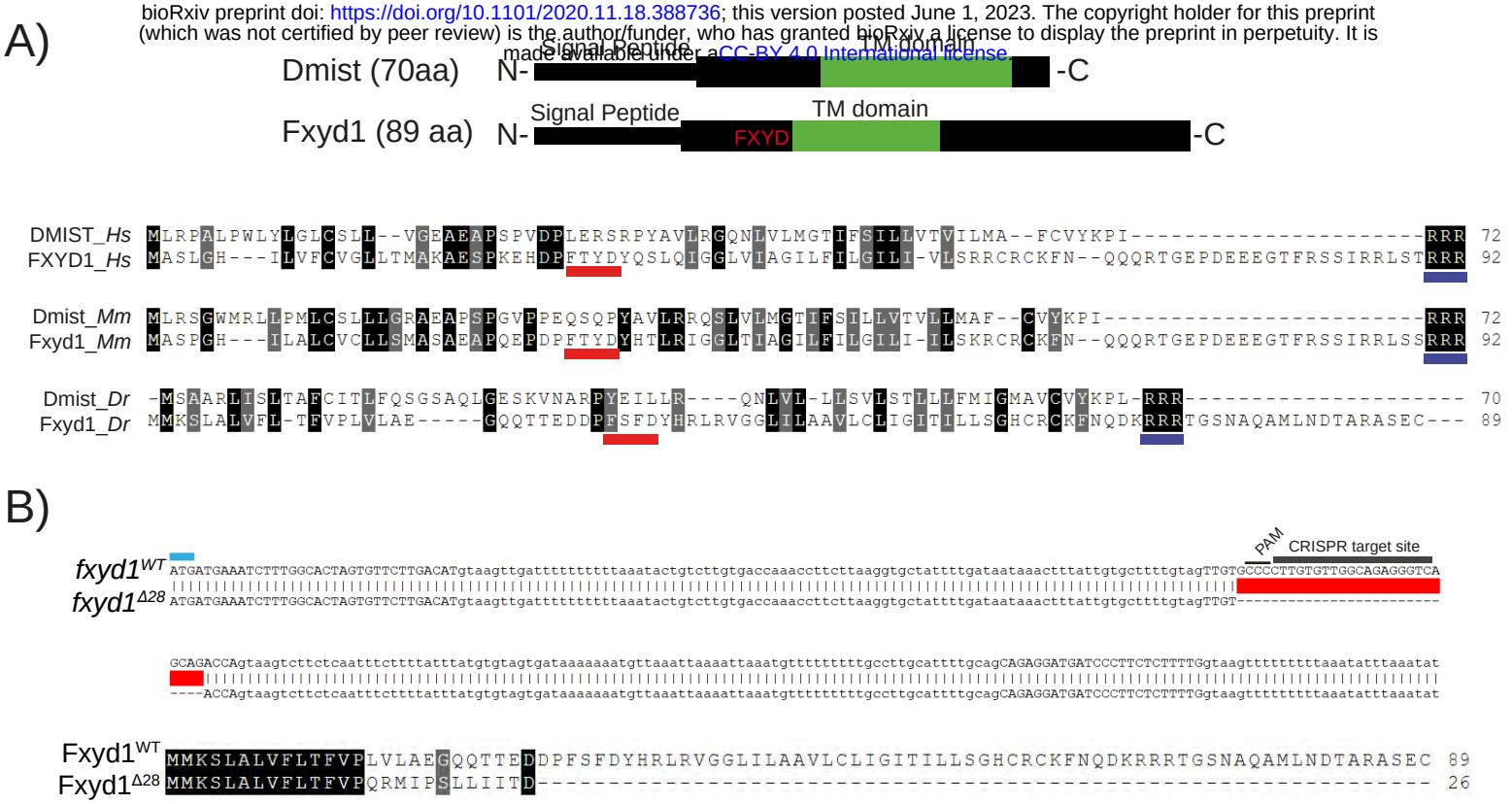

Figure 4

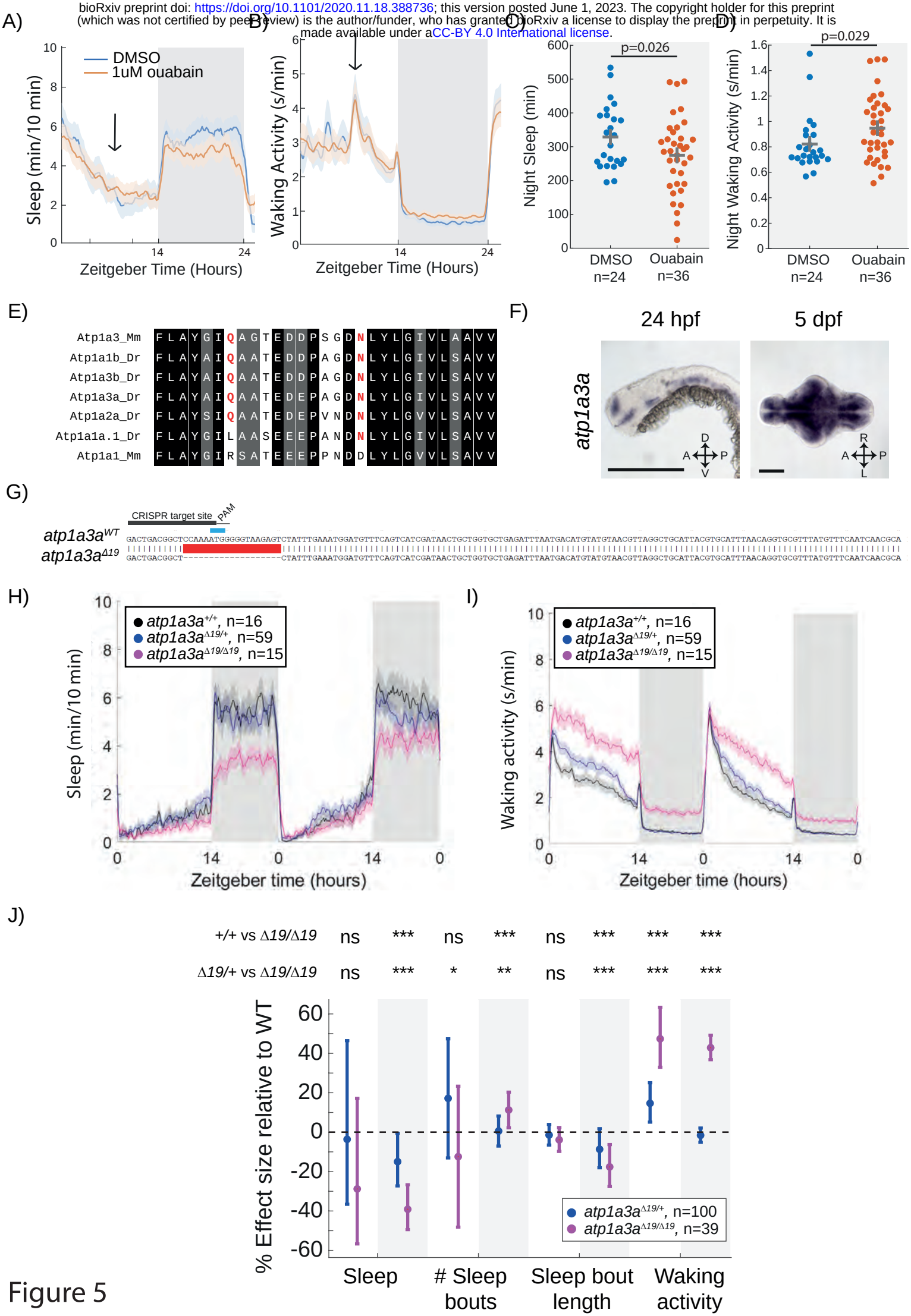

Figure 5

A)

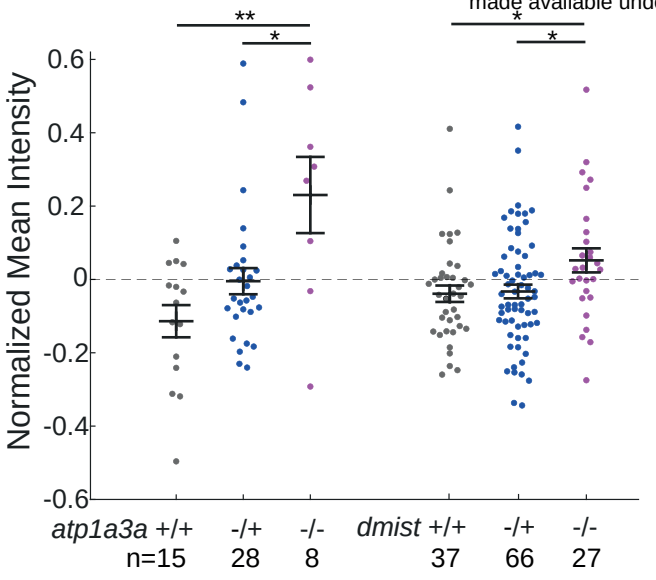

B)

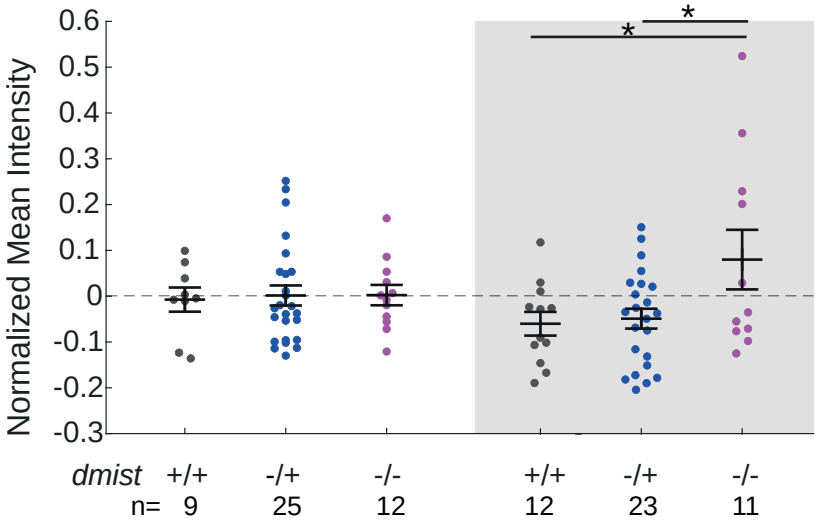

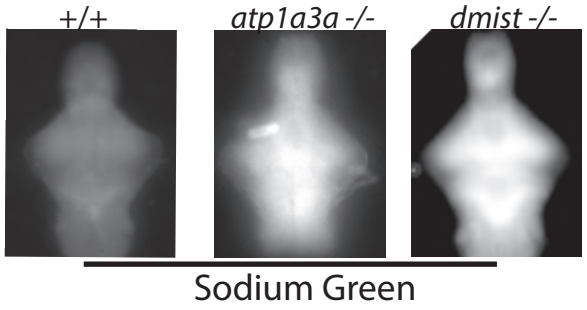

C)

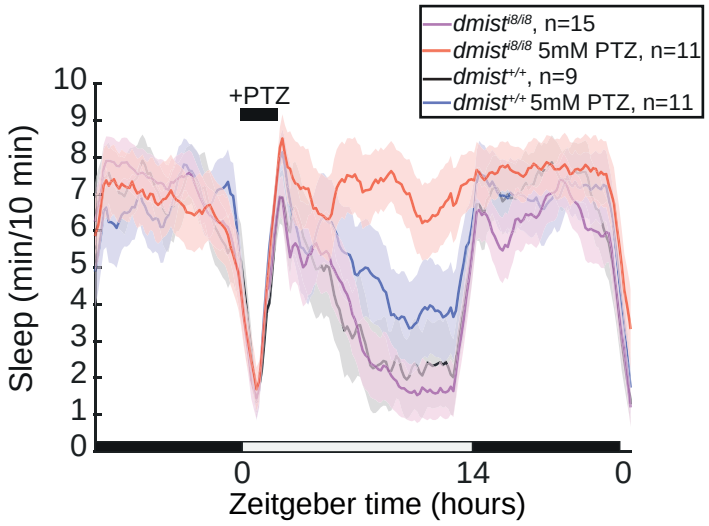

D)

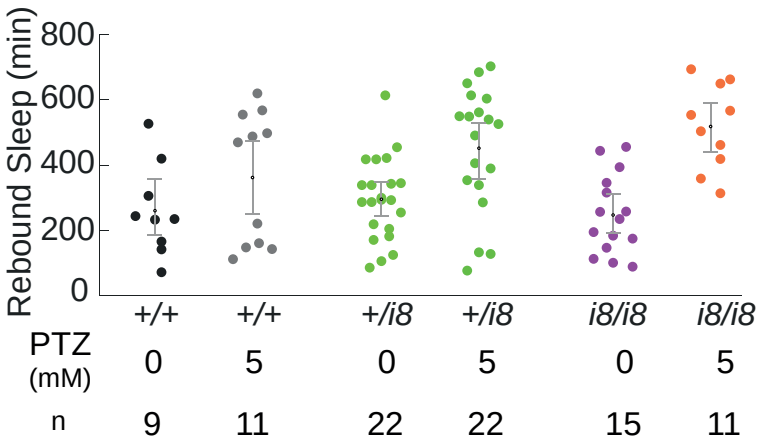

E)

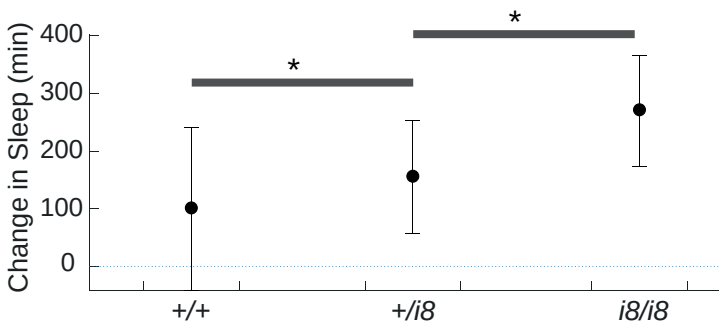

F)

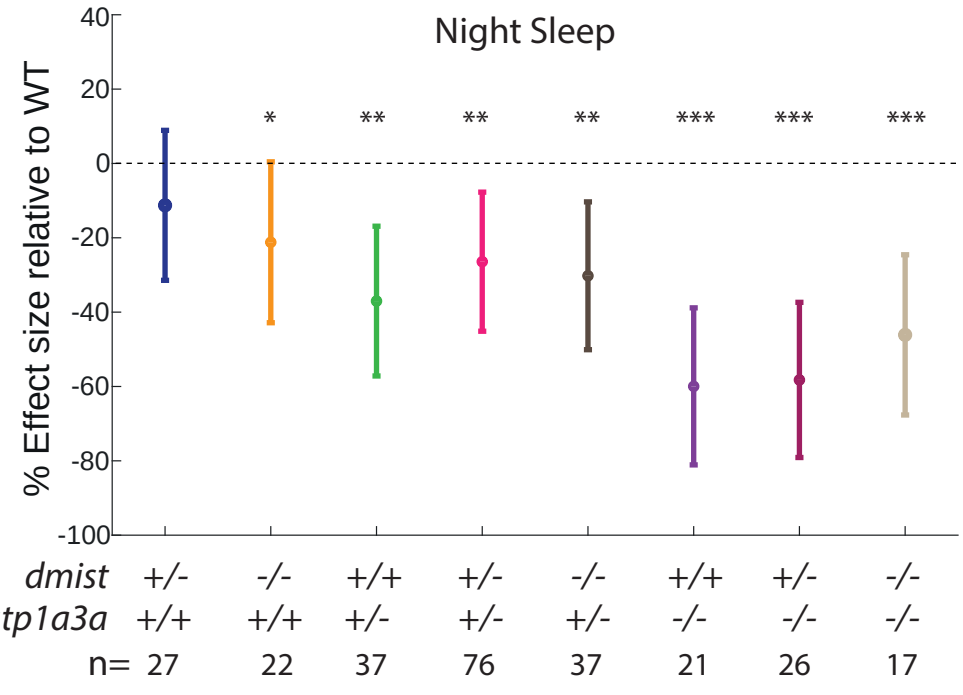

Figure 6

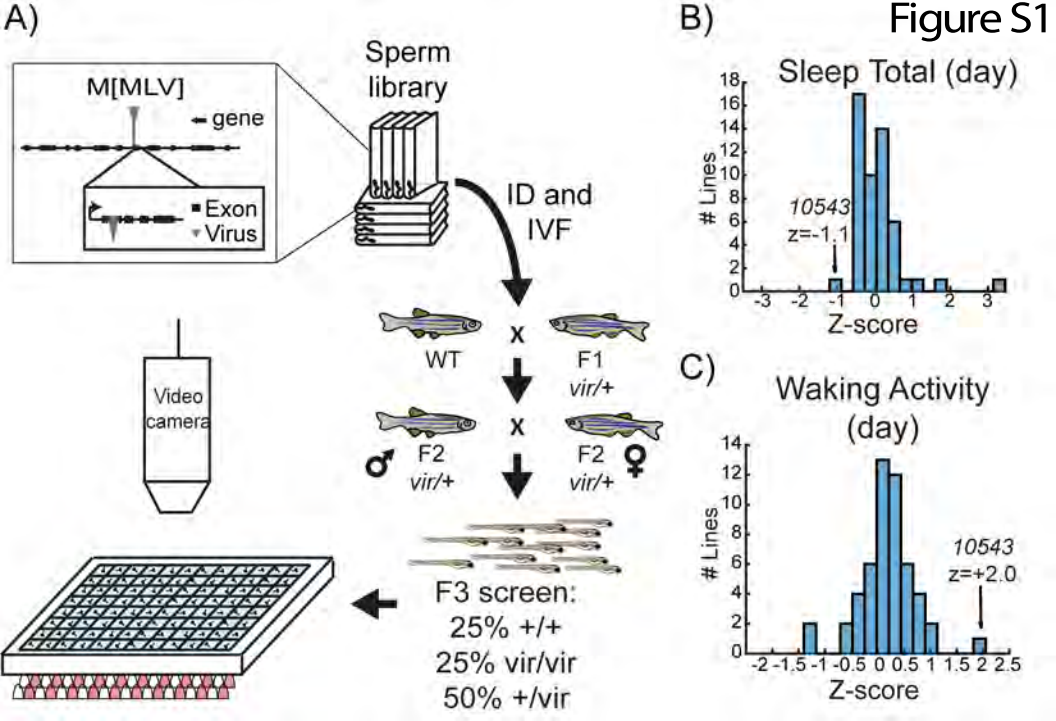
A)
M[MLV]
gene
Exon
Virus
Sperm library
ID and IVF
WT
x
F1
vir/+
Video camera
F2
vir/+
x
F2
vir/+
F3 screen:
25% +/+
25% vir/vir
50% +/vir
B)
Sleep Total (day)
Lines
10543
z=-1.1
Z-score
C)
Waking Activity (day)
Lines
10543
z=+2.0
Z-score

Figure S1

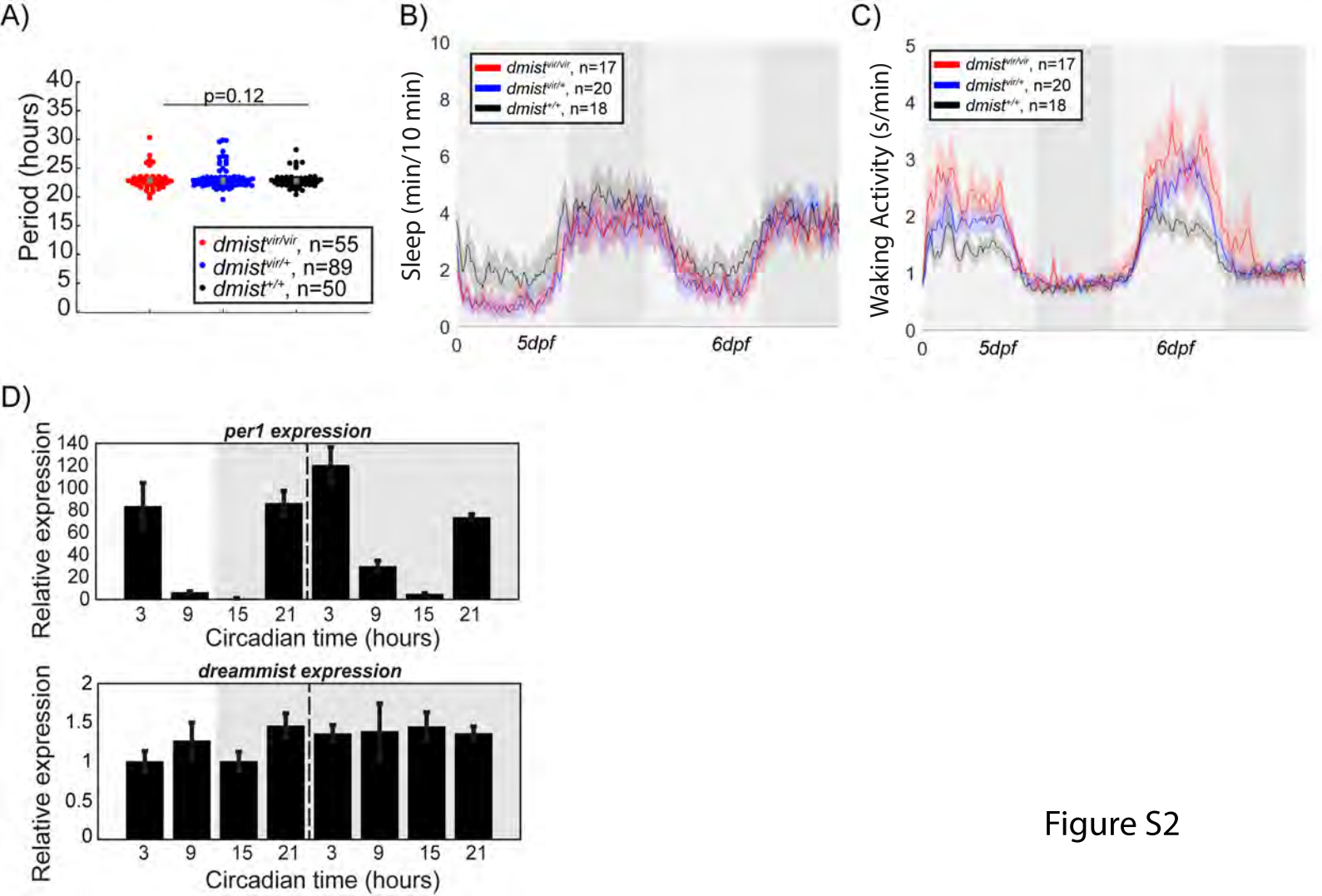
A)
Period (hours)
p=0.12
dmist^vir/vir, n=55
dmist^vir/+, n=89
dmist+/+, n=50
B)
Sleep (min/10 min)
dmist^vir/vir, n=17
dmist^vir/+, n=20
dmist+/+, n=18
5dpf
6dpf
C)
Waking Activity (s/min)
dmist^vir/vir, n=17
dmist^vir/+, n=20
dmist+/+, n=18
5dpf
6dpf
D)
per1 expression
Relative expression
Circadian time (hours)
dreammist expression
Relative expression
Circadian time (hours)

Figure S2

Figure S3

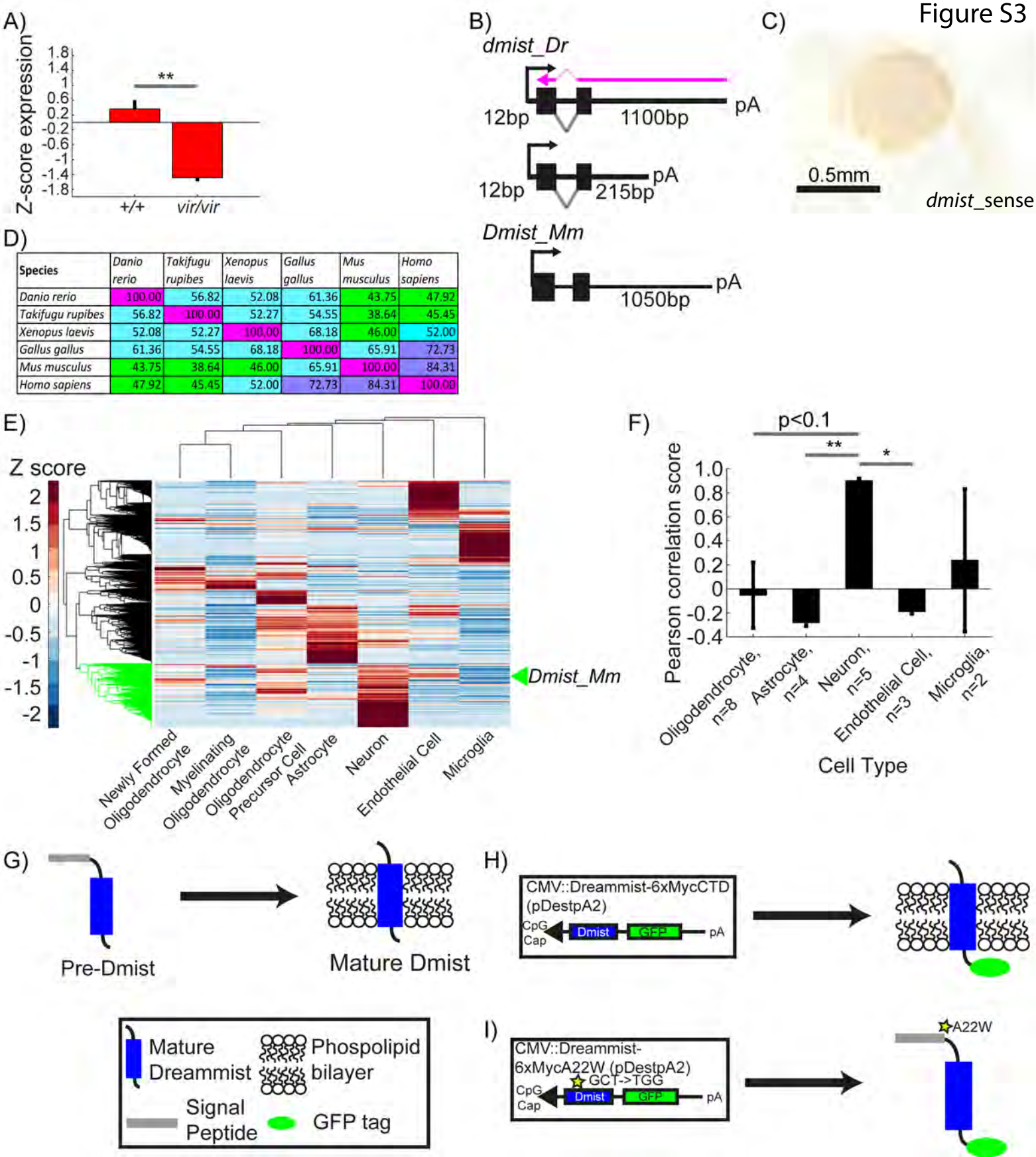

Species	*Danio rerio*	*Takifugu rupibes*	*Xenopus laevis*	*Gallus gallus*	*Mus musculus*	*Homo sapiens*
Danio rerio	100.00	56.82	52.08	61.36	43.75	47.92
Takifugu rupibes	56.82	100.00	52.27	54.55	38.64	45.45
Xenopus laevis	52.08	52.27	100.00	68.18	46.00	52.00
Gallus gallus	61.36	54.55	68.18	100.00	65.91	72.73
Mus musculus	43.75	38.64	46.00	65.91	100.00	84.31
Homo sapiens	47.92	45.45	52.00	72.73	84.31	100.00

A)

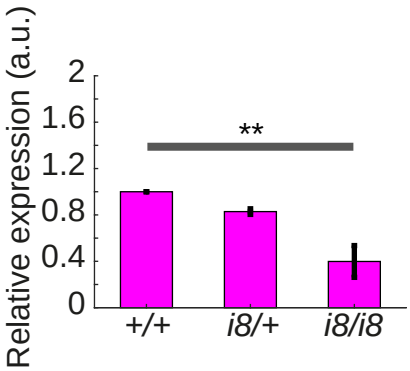

B)

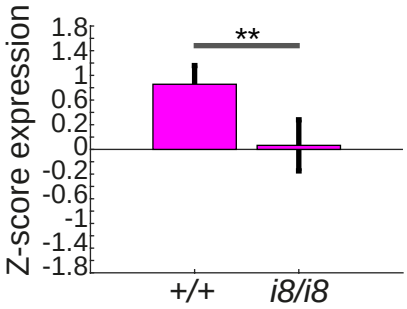

Figure S4

A)

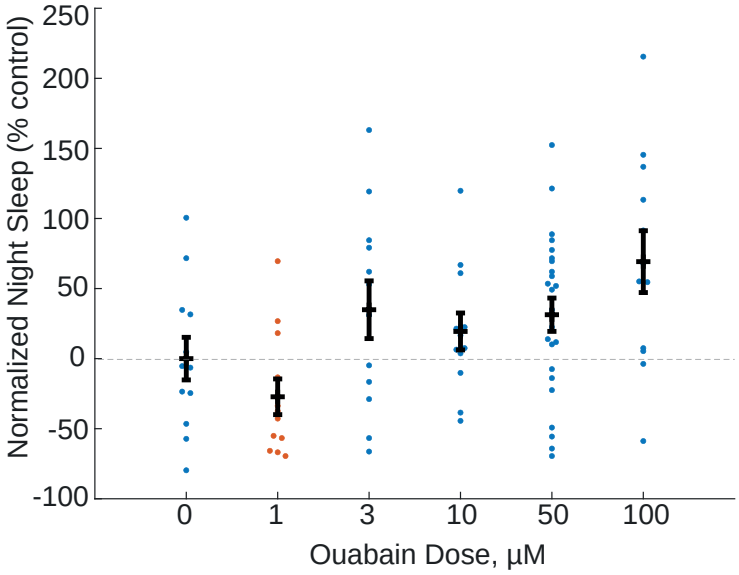

B)

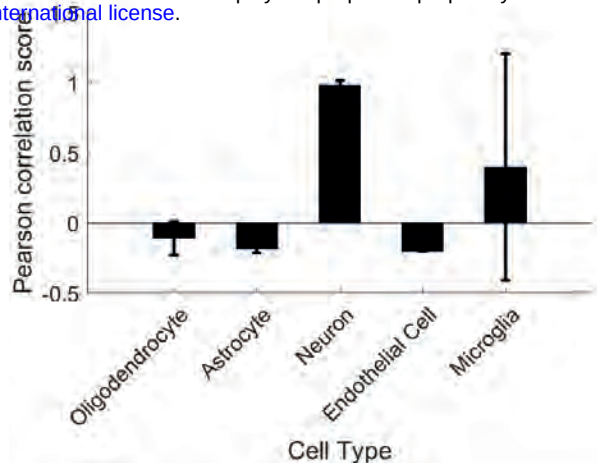

C)

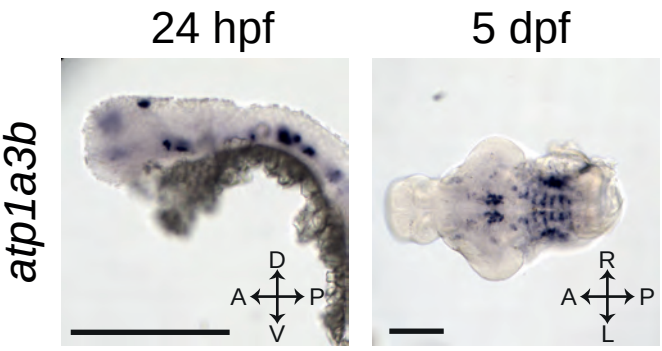

D)

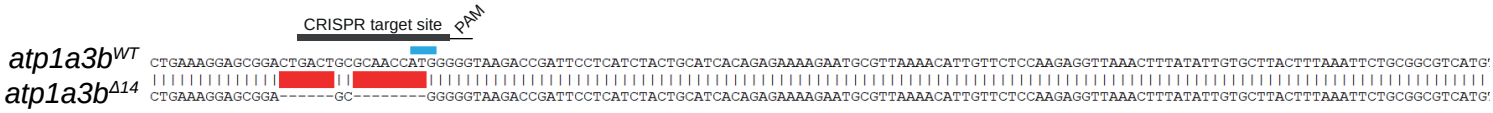

E)

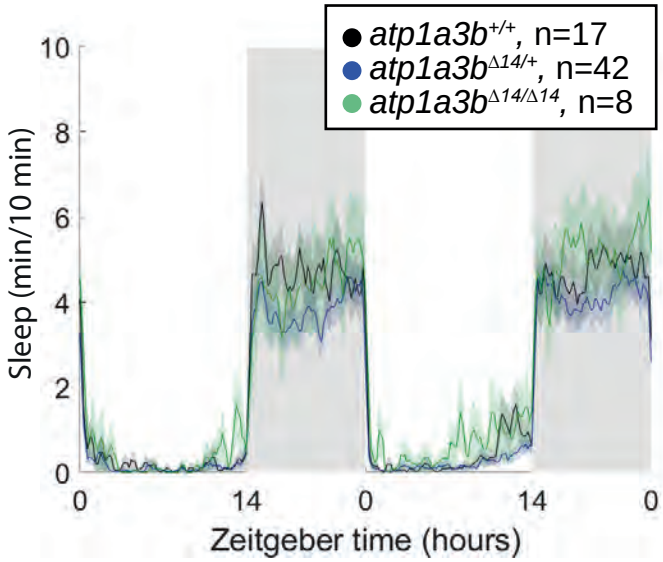

F)

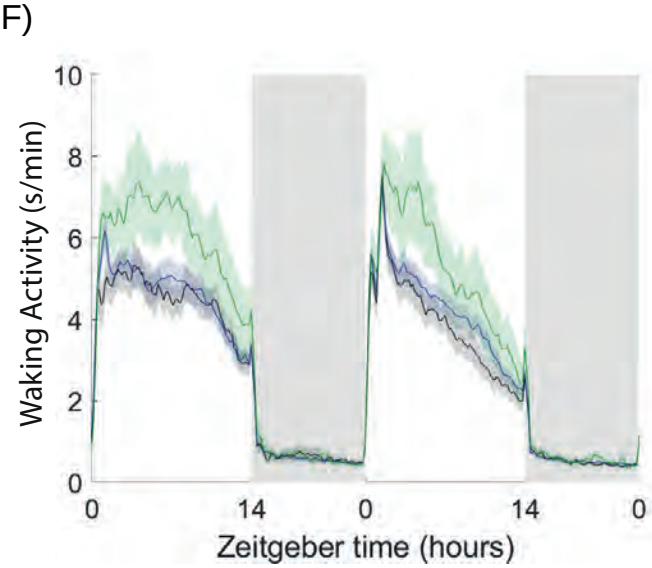

G)

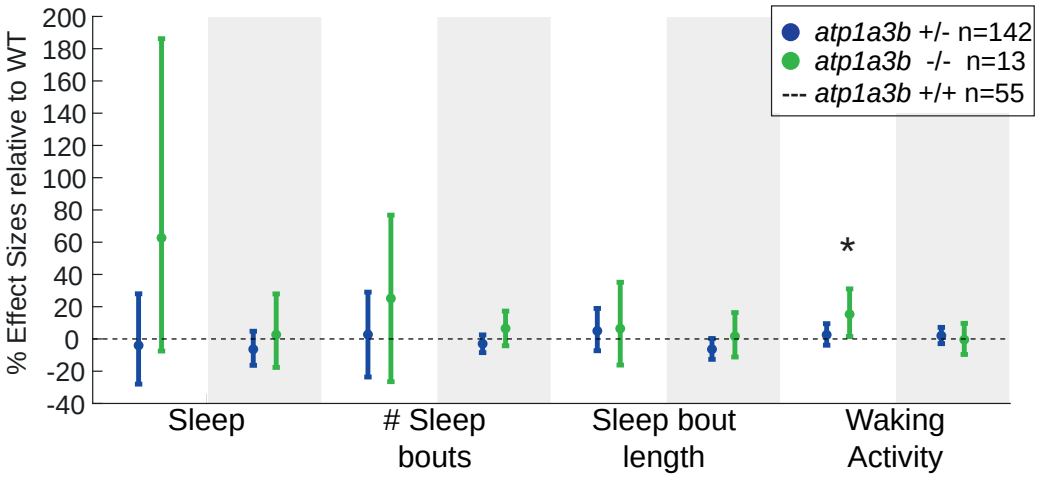

Figure S5

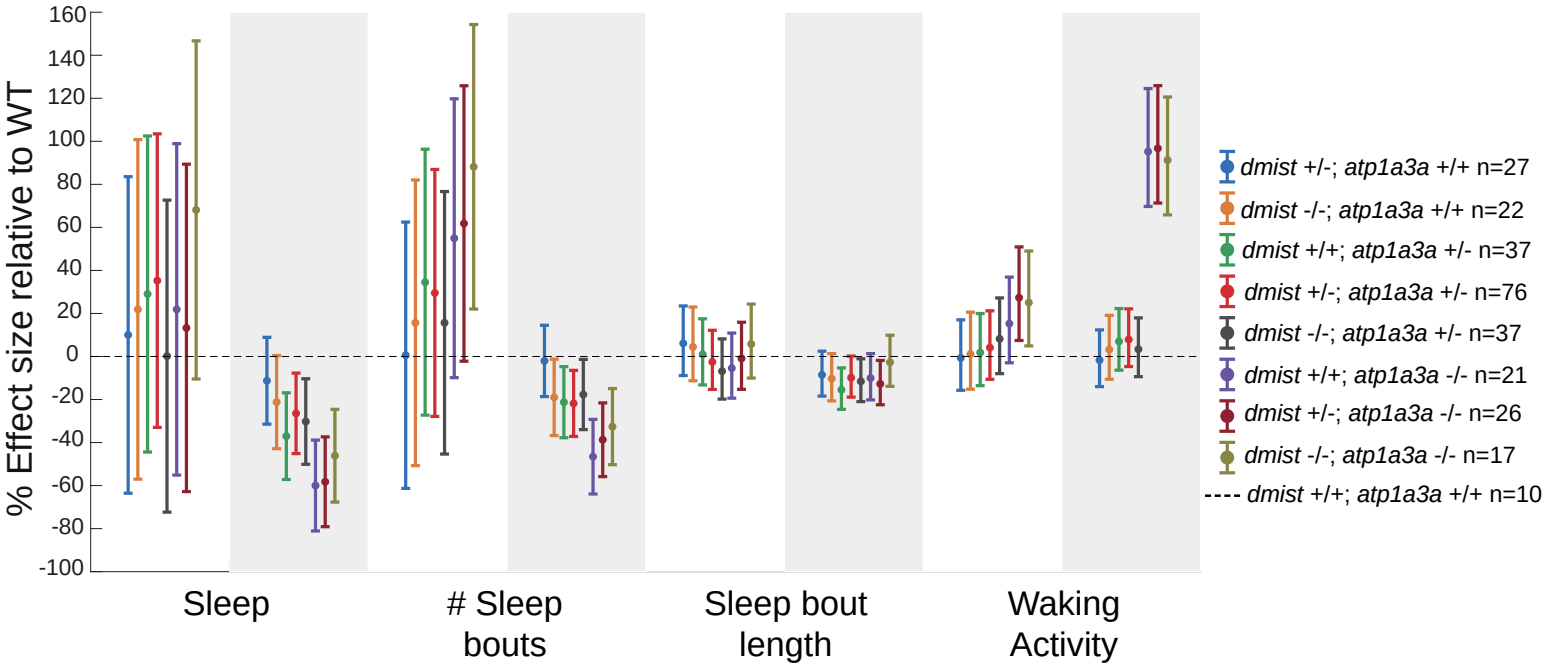

Figure S6